PROGRESS REPORT
Grant NGL 34-002-047
October 15, 1969

"STUDY OF RECTANGULAR-GUIDE-LIKE STRUCTURES FOR MILLIMETER WAVE TRANSMISSION"

to
The National Aeronautics and Space Administration, Washington, D. C.

DEPARTMENT OF ELECTRICAL ENGINEERING
NORTH CAROLINA STATE UNIVERSITY
RALEIGH, NORTH CAROLINA

PROGRESS REPORT
Grant NGL 34-002-047
October 15, 1969

"STUDY OF RECTANGULAR-GUIDE-LIKE STRUCTURES FOR MILLIMETER WAVE TRANSMISSION"

to
The National Aeronautics and Space Administration, Washington, D. C.

North Carolina State University
Raleigh, North Carolina

Submitted: Frederick J. Tischer

Dr. Frederick J. Tischer, Professor
Principal Investigator

PERSONNEL

Dr. Frederick J. Tischer, Principal Investigator

Dr. Makato Itoh, Visiting Professor of Mathematics

Mr. Lyles Adair, Graduate Student

Mr. K. K. Agarwal*, Graduate Student

Mr. I. H. Chen, Graduate Student

Mr. F. Jalali, Graduate Student

Mr. R. A. Kraft, Undergraduate Assistant

* Mr. Agarwal joined the Laboratory September 1, 1969

TABLE OF CONTENTS

INTRODUCTION

This progress report presents results of research carried out under Grant NGL 34-002-047 during the period June 1 through September 30, 1969.

During the report period a paper entitled, "H-Guide with Artificial and Laminated Dielectric Slabs," was presented by the Principal Investigator at the 1969 European Microwave Conference, 8-12 September, in London, England. A report on the conference was prepared and distributed as a special item during the latter part of September. The discussions following the presentation of the paper indicated considerable interest in the topic since millimeter waves are considered the most promising frequency region for an extension of the present communications facilities taking into consideration the large volume of information necessary to be carried in the near future. Recent progress in the development of new solid state generators (bulk-effect devices) for this frequency region and of low-loss materials make the use of millimeter waves very practical. H-guide and fence guide offer attractive solutions of millimeter wave circuit problems and transmission problems.

Prior to the conference, visits were made to the University of Sheffield and at the University College in London. At both universities extensive research and design studies are carried out in the microwave and millimeter wave region. A brief account of this research will be given as an Appendix to the Introduction. The work on the effects of surface roughness on the attenuation

of waveguides is of particular interest in connection with our study. These effects were extensively investigated in Sheffield primarily at 10 GHz and they are under investigation in our laboratory at 35 GHz and above. In this frequency region the effects are more pronounced than in the former and any improvements correspond to a considerable amount of savings in transmitted power or number of repeater stations.

The structures under investigation in our laboratory are (a) the fence guide, (b) the H-guide with laminated dielectric, and (c) the beam guide. Of these structures, (a) is primarily suited for the design of millimeter-wave circuitry and (b) and (c) for low-loss transmission. The fence guide is investigated experimentally and theoretically for the determination of its characteristics, for the derivation of design parameters and corresponding relationships, and with regard to incorporation of components.

New transitions between rectangular waveguides on one hand and fence guides and H-guides on the other, were designed and manufactured since the original devices were found to introduce excessively undesired wave modes. The characteristics of the new transitions (field distribution in front of the horn-type transitions) were measured and found in agreement with the predictions. Part 5 of this report presents the results of the measurements. A section of the fence guide in combination with the new transitions is now under experimental investigation. The field distribution inside the guide and in its vicinity are

measured by capacitive and inductive probes to verify and to complement the results of the theoretical study underway.

The measurement of the field distribution turnes out to be a rather delicate problem as distortions of the measured fields by the probing devices have to be avoided. The probes must have rather small sizes at 35 GHz to achieve this goal. Measurements by the use of specially designed capacitive and inductive probes are being made.

The study of a confocal circular reflector guide was continued during the report period. This guide may be considered as an oversized, two-wall waveguide with characteristics similar to those of the H-guide. The confinement of the field in one cross-sectional direction is achieved by the curved form of the conducting side walls. The section of this report on this guide deals primarily with the contribution to the attenuation by radiation from the upper and lower opening. The power loss is determined by considering the openings of the guide as radiating surfaces. Relationships are derived which show the contributions to the attenuation by wall losses and radiation in terms of the cross-sectional dimensions and of the angle under which the waves are injected into the guide. An experimental prototype of a short section of such a guide including end plates to form a resonator has been manufactured and will be investigated. Relationships for the computation of the Q-value of the resonator under investigation are also shown in the report.

Part 4 of this report deals with the effects of surface roughness on the loss-characteristics of waveguides. These effects are particularly important in the case of H-guides and beam waveguides since their surfaces are readily accessible to surface treatment. Values of the attenuation up to 50% above the theoretical values were observed at millimeter waves so that prediction and improvement of the attenuation is an important problem in the upper-frequency regions.

Methods for the correlation and for the non-destructive measurement of the roughness will be developed. Simultaneously procedures recommended for the improvement of the surface resistance will be tested. The results of research carried out at the University of Sheffield indicate that considerable improvements of the loss characteristics can be achieved by electro and chemical polishing. The work by Russian scientists studying the influence of the micro structure of the current-carrying layers led to similar conclusions. Results of their work were presented in abstract form at the European Microwave Conference.

Dr. Makato Itoh participated during the first part of the summer in the research of the laboratory. He has recently developed methods of the description of electromagnetic fields by wave-analytic functions and has derived relationships which can be applied for the solution of boundary value problems related to guided waves. As a first part, algebraic relationships for a commutative bicomplex number system were presented in the preceding progress report. The study is continued in

the present report with a comparison of the characteristics of analytic and wave-analytic functions. In a third part to be included in a later report, the application of bicomplex wave analytic functions to relationships typical for uniform electromagnetic-wave transmission will be discussed.

PAPER PRESENTED AT THE
EUROPEAN MICROWAVE CONFERENCE
SEPTEMBER 8 - 12, 1969
LONDON, ENGLAND

H-GUIDES WITH ARTIFICIAL AND LAMINATED DIELECTRIC SLABS

by F. J. Tischer

One of the more sophisticated non-conventional waveguides with a considerable potential for application at millimeter waves is the H-guide. In this hybrid waveguide, the fields are concentrated in one transverse direction by surface-wave propagation along a dielectric slab and are confined in the other direction by parallel conducting planes. The cross section has the form of an H with the conducting side walls forming its vertical legs and the dielectric slab the horizontal bar. The guide has low conduction losses similar to those of the waveguide with circular cross section for TE_{10} waves. The major contribution to the attenuation results from dielectric losses in the central dielectric bar. Using regular dielectrics, the attenuation constant becomes relatively high. Measures to reduce the dielectric losses such as by lamination of the dielectric were proposed already in early publications.

A more recent approach is based on the use of artificial dielectrics. Such dielectrics consist of highly conducting metallic structures with dimensions small in comparison with the wavelength which have the same effect as a solid dielectric.

Dr. Tischer is Professor at the North Carolina State University, Raleigh, North Carolina, U.S.A. This work was supported by the National Aeronautics and Space Administration.

Examples are metallic strips, spheres, and cylinders embedded in a low-loss, low-permittivity, foamed dielectric. By using such a structure, the dielectric losses can be practically eliminated. The total attenuation of the guide can then be kept at a low level by optimization of the geometry. An example of an H-guide with a strip structure as artificial dielectric is shown in Fig. 1. The strips confine the fields to a region near them as does the solid dielectric bar of the conventional guide.

The fields decrease exponentially from the center toward the upper and lower openings. Relationships for the field components can be found by writing general expressions for the fields within and above the strip structure and by matching the amplitudes at the boundary between the two regions. The different sets of expressions are required to be identical at the boundary, $x = a$. Only the fundamental terms of the infinite series contribute to the basic H-guide fields if the distances between the strips are much smaller than the wavelength. The zero-order field above the strip structure is given by

$$E_z = a \cos(k_y y) \exp(-\alpha_x x) \exp(-jk_z z) \quad ,$$

$$E_x = (jak_z/\alpha_x) \cos(k_y y) \exp(-\alpha_x x) \exp(-jk_z z) \quad ,$$

$$E_y = 0 \quad ,$$

$$H_x = (-jk_y a/\omega\mu) \sin(k_y y) \exp(-\alpha_x x) \exp(-jk_z z) \quad ,$$

$$H_y = ja(\alpha_x^2 - k_z^2)/(\omega\mu\alpha_x) \cos(k_y y) \exp(-\alpha_x x) \exp(-jk_z z) \quad ,$$

$$H_z = (ak_z k_y)/(\omega\mu\alpha_x) \sin(k_y y) \exp(-\alpha_x x) \exp(-jk_z z) \quad ,$$

where the propagation constants are related by

$$\alpha_x^2 - k_y^2 - k_z^2 + k^2 = 0 \quad , \qquad k_y = \pi/b \quad ,$$

$$\alpha_x = [(k^2 - k_y^2) \tan(ka)]/k \quad , \qquad k^2 = \omega^2\mu\varepsilon \quad .$$

It is interesting to note that the component E_y vanishes, whereas H_x vanishes for the conventional H-guide. The attenuation of the guide can then be computed from the power losses and the power transmitted by using the field equations. The attenuation can be separated into three components, $\alpha = \alpha_{wa}+\alpha_{ns}+\alpha_s$, where the components are respectively that due to losses in the side walls above and within the region of the strip structures, and on the strips themselves. Numerical values of the total attenuation evaluated at frequencies of 35 and 70 GHz are shown graphically in Figs. 2a and 2b. It is noted that for a value of $p = \alpha_x/k_o = .2$ which corresponds to a 90% decrease of the field at a distance of $x = 2\lambda$, the attenuation is about 1/10 of that of the standard rectangular waveguide.

Lamination is another approach by which the loss characteristics can be improved. This was shown in studies of an H-guide with double dielectric slabs. Several authors[1,2,3] reported results. In more recent studies, subdivision of the dielectric slab into an arbitrary number of dielectric strips separated by air layers was investigated.[4] The slab structure may be considered as an artificial dielectric with the characteristics described by an equivalent permittivity and loss tangent. An example of such a guide is illustrated in Fig. 1b.

The computation of the field distribution in such a guide can be considerably simplified by considering the fields as those of superimposed plane surface waves reflected between the side walls. The computation can then be carried out in two parts, one dealing with propagation along an infinitely wide laminated slab and the other dealing with the superposition of the plane surface waves.

The final results are sets of equations for the various regions of the following general form:

$$H_z^{(n)} = (k_y/k_\ell)[U_n c(x)+jV_n s(x)]\cos(k_y y)\exp(-jk_z z) \quad ,$$

$$H_y^{(n)} = (jk_z/k_\ell)[U_n c(x)+jV_n s(x)]\sin(k_y y)\exp(-jk_z z) \quad ,$$

$$E_z^{(n)} = (k_\ell/\omega\varepsilon_o\varepsilon_r)[U_n c(x)+jV_n s(x)]\sin(k_y y)\exp(-jk_z z) \quad ,$$

$$E_y^{(n)} = (k_x k_y/\omega\varepsilon_o\varepsilon_r k_\ell)[V_n c(x)-jU_n s(x)]\cos(k_y y)\exp(-jk_z z) \quad ,$$

$$E_z^{(n)} = (-jk_x k_z/\omega\varepsilon_o\varepsilon_r k_\ell)[V_n c(x)-jU_n s(x)]\sin(k_y y)\exp(-jk_z z) \quad .$$

The functions c(x) and s(x) stand for trigonometric functions within the strips, hyperbolic functions in the air layers, and exponential functions above the slab. The constants U_n and V_n are obtained from the field components at the lower boundary of the region under consideration.

The evaluation of these equations and the resulting relationships are particularly interesting in the case of thin dielectric and air layers. The following relationships are obtained for the equivalent permittivity and loss tangent,

$$\varepsilon_{req} \simeq \varepsilon_r(1+p/\varepsilon_r)/(1+p) \quad ; \quad \tan\delta_{eq} \simeq \tan\delta/(1+p\varepsilon_r) \quad ,$$

where ε_r and tan δ are the constants for the material of the strips and $p = d_a/d_\varepsilon$ represents an air-to-dielectric thickness ratio. Investigation of available materials shows that lamination leads to very low values of the equivalent loss tangent. Examples of approximate equivalent parameters for a few materials are shown in Table 1. It is expected that use of laminated slabs will result in considerable improvements over conventional rectangular waveguides.

References

1 Tischer, F. J., Properties of the H-Guide at Microwave and Millimeter Wave Regions, Proc. IEE, 106, Part B, Suppl. No. 13, pp. 47-53 (1959).

2 Conlon, R. F. D., and Benson, F. A., Propagation and Attenuation in the Double-Strip H-Guide, Proc. IEE, 113, No. 8, pp. 1311-1320 (1966).

3 Deniskin, YU. D., Metal-Dielectric H-Guide with Two Dielectric Slabs, Telecomm. Radio Engng., 18, p. 37 (1963).

4 Tischer, F. J., H-Guide with Laminated Dielectric, Proc. IEEE, 57, No. 5, pp. 820-821 (May 1969).

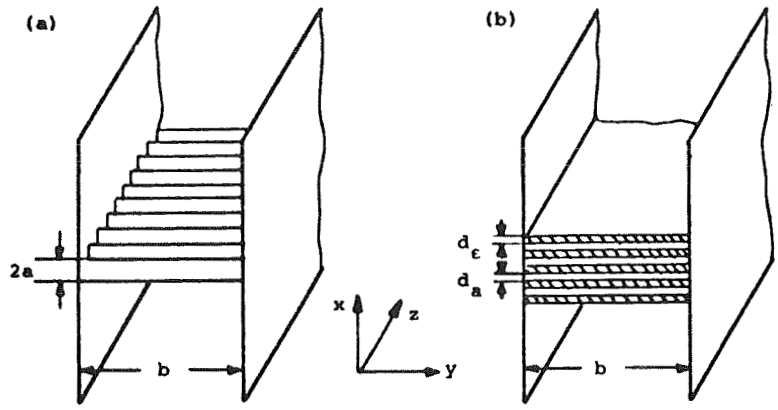

Fig. 1 Hguide with artificial dielectrics
(a) With strip structure
(b) With laminated dielectric

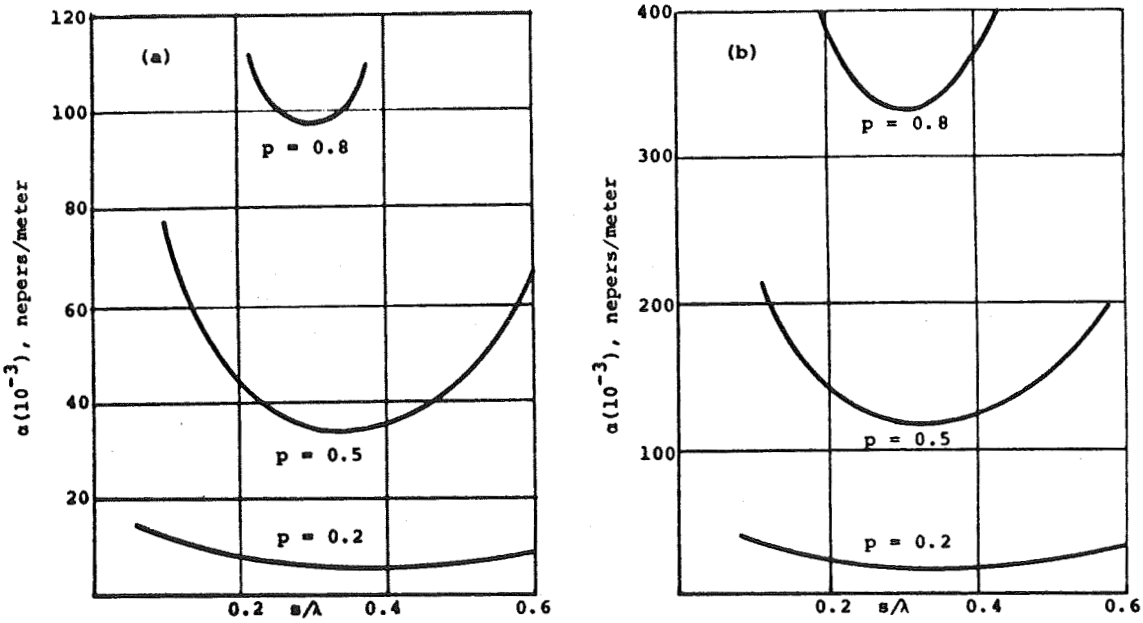

Fig. 2 Attenuation of Hguide with strip structure with 0.0286 m sidewall spacing
(a) 35 GHz ; (b) 70 GHz

Table 1. Laminated slab parameters

	Single slab medium constants		Equivalent medium constants		
Dielectric	ϵ_r	tan δ	p	$\epsilon_{r\ eq}$	tan δ_{eq}
Styrofoam	1.03	1.5×10^{-4}			
Rexolite	2.53	7.0×10^{-4}*	7.5	1.16	3.5×10^{-5}
Beryllium Oxide (99.5%)	6.6	4.4×10^{-4}	3	2.4	2.6×10^{-5}
Aluminum Oxide (99.9%)	9.9	2.5×10^{-5}	5	2.5	5.0×10^{-7}
Eccoceram	90	1.0×10^{-3}	10	9.0	1.1×10^{-6}

VISITS AT THE UNIVERSITY OF SHEFFIELD AND UNIVERSITY COLLEGE, LONDON

Visits at the above two universities and discussions with participants at the conference revealed considerable activities in the area of microwaves and millimeter waves in industry, government laboratories, and at the universities. The Electrical Engineering Department of the University of Sheffield is a typical example where at present about thirty research projects are underway. Examples of some of the topics are phase-locking of Gunn oscillators, effects of geometry variations on the characteristics of waveguides, active antenna arrays, Gunn-effect devices in fast computers, amplification mode of the Gunn effect, microwave holography, and effects of surface roughness on the attenuation of waveguides.

Studies of a double-slab H-guide and of the surface roughness were of particular interest from a viewpoint of the work at our laboratory. It was found in Sheffield that the attenuation of the H-guide can be reduced by about 40% by subdividing the central slab of the H-guide into two strips. This confirms the results of studies carried out by the principal investigator in a previous study.

The conclusions drawn from the study of the surface roughness seem to indicate that the primary origin of the increase in attenuation of drawn waveguides at X-band and A-band (35 GHz) frequencies is the surface roughness. This

conclusion was drawn on the basis of studies of the surface by using a scanning electron beam microscope. The pictures obtained by this instrument, which has an extra-ordinary depth of perception, indicate the presence of cavity-type holes which considerably affect the current flow. Computer programs for the determination of the attenuation taking into account such cavity-type surface deformations indicated increases of the attenuation by factors up to 1.8. It was concluded that electro-physical surface effects play a minor role.

The studies also showed that improvements of the attenuation can be obtained by chemical polishing and electro polishing. The ratios of measured and theoretical attenuations for surfaces treated in this way were better than 1.02 in some cases. Whether this reduction is the result of changes of the surface geometry only is difficult to asses.

Another study deals with the effects of geometry changes on the characteristics of waveguides and components. It is very thoroughly carried out and a great variety of components such as impedance transformers, directional couplers, hybrids, terminations, etc., are under investigation.

The use of the Gunn effect in computers deserves particular attention since it opens the way for the generation of ultra-short pulses and thus the development of ultra-fast computers. Pulse generators, gates, and pulse re-generators are under development and study. The generation of high-power pulses by switching the cavity of a cavity-controlled Gunn oscillator is another novel idea under investigation well worth mentioning.

The Department of Electronic and Electrical Engineering of the University College, London, has an extensive research program also. Millimeter-wave guides, transitions between different types of guides, dielectric-rod waveguides, transmission by over-moded rectangular waveguides, long-distance transmission by circular waveguides, measurement setups for the study of dielectrics at millimeter waves are among the topics under investigation.

The objective of a study of transitions between different types of waveguides is to achieve complete power transfer by quasi-periodic mode coupling. Extremely wide-band performance was obtained in preliminary studies. Another project deals with the characteristics of tapered dielectric waveguides. The computations are carried out by perturbation methods. The possibility to transmit millimeter wave energy with low attenuation for wide frequency bands over long distances is being studied. Emphasis is placed on the behavior of a dielectric-coated circular waveguide which is considered to be superior to the regular circular waveguide. A special confocal spherical resonator is being used at 10 GHz for the non-destructive determination of the characteristics of dielectrics in the form of thin slabs. The method eliminates the machining of the material under investigation into specific shapes.

In general, it should be mentioned that students and faculty are very enthusiastic about their work and their accomplishments, the instrumentation is very good with latest equipment in use. The work is financed in part by scholarships, by

the ministry of defense, the ministry of technology, and, to a larger part than in the United States, by industry.

Part 2

ON THE COMPUTATION OF THE ATTENUATION OF H-GUIDES AND FENCE GUIDES

Abstract

This paper deals with a comparison of two methods for the computation of the attenuation of surface-waveguides, for which the H-guide and fence guide are examples. Evaluation of transmitted and dissipated power for field distributions of the loss-less guide is the basis of one method, use of the characteristic equation leads to the other. The conditions under which both methods give equal results are considered and formulated. The problem becomes important in the case of the fence guide and in the case of the H-guide with incorporated circuit elements when losses and energy sources are no longer negligible.

ON THE COMPUTATION OF THE ATTENUATION OF H-GUIDES AND FENCE GUIDES

Introduction

Two methods are commonly used for determination of the attenuation in waveguides. One of these methods is based on the familiar relationship

$$\alpha_z = P_L/2P_T$$

where α is the attenuation constant and P_L and P_T are power loss and power transported per unit length of the waveguide, respectively. The power calculations are made on the basis of field distributions obtained under the assumption of zero losses which is acceptable for most practical waveguides. Thus, given the field components and the geometry of the waveguide, the attenuation can be easily determined by computing the power transported and power lost. The second method consists of solving one or several characteristic equations associated with the waveguide to obtain the imaginary part of the field distribution constant in the direction of propagation which represents the attenuation.

The question arises then whether or not the two methods give agreeing results. It is usually assumed that they do. A study of the attenuation in H-guides shows this not to be true in general. In the following sections, expressions for the attenuation are derived by both methods and the necessary conditions determined for their agreement. The losses in the dielectric will be considered only which corresponds to conditions of an infinite-width H-guide.

Attenuation Computed by the Power Method

Here we shall consider quasi-TM waves. Since the width is infinite, the field in the y-direction is constant, $k_y = 0$. The field components in the region outside the dielectric are[1]

$$E_z = E_o\, e^{-\alpha_x(x-d)}\, e^{-jk_z z} \quad ,$$

$$E_x = \frac{-jk_z}{\alpha_x}\, E_o\, e^{-\alpha_x(x-d)}\, e^{-jk_z z} \quad ,$$

$$H_y = \frac{-j\omega\varepsilon_o}{\alpha_x}\, E_o\, e^{-\alpha_x(x-d)}\, e^{-jk_z z} \quad ,$$

and inside the dielectric,

$$E_z = E_1 \sin k_x x\, e^{-jk_z z} \quad ,$$

$$E_x = \frac{-jk_z}{k_x}\, E_1 \cos k_x x\, e^{-jk_z z} \quad ,$$

$$H_y = \frac{-j\omega\varepsilon}{k_x}\, E_1 \cos k_x x\, e^{-jk_z z} \quad .$$

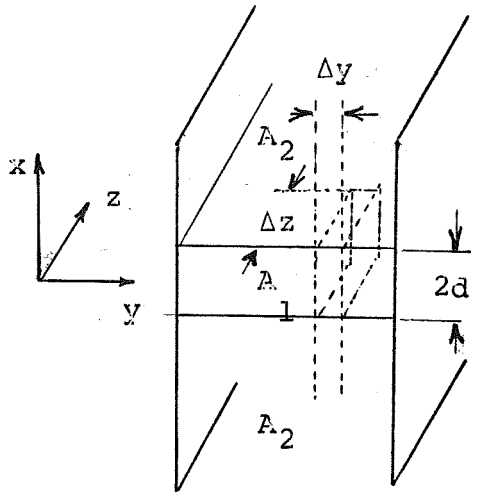

Fig. 2.1 Guide Geometry

The total transported power is the sum of the powers transported in the dielectric and air regions; see Fig. 2.1.

$$P_T = \frac{1}{2} \int_{A_1+A_2} \mathrm{Re}\,[E_x \times H_y^*]\, dA$$

The integrals for the two regions become

$$P_T = \frac{1}{2}\, \frac{\omega\varepsilon k_z}{k_x^2}\, E_1^2 \left(d + \frac{\sin 2k_x d}{2k_x}\right) + \frac{1}{2}\, \frac{\omega\varepsilon_o k_z}{\alpha_x^3}\, E_o^2 \quad .$$

Field matching at the boundary of dielectric and air yields[1]

$$E_o = E_1 \sin k_x d \quad .$$

The total transported power is then given by

$$P_T = \frac{\omega\varepsilon\, k_z\, E_1^2}{2}\left[\frac{1}{k_x^2}\left(d + \frac{\sin 2k_x d}{2k_x}\right) + \frac{\sin^2 k_x d}{\varepsilon_r\, \alpha_x^3}\right] .$$

Since the losses are due to the dielectric only, the power loss per unit length becomes

$$P_L = \frac{1}{2}\int \sigma|E|^2\, dv$$

$$= \frac{1}{2}\int_{-d}^{d}\left[\left(\frac{k_z}{k_x}\right)^2 E_1^2 \cos k_x x\, d_x + E_1^2 \sin^2 k_x x\, dx\right] \Delta y\, \Delta z \quad ,$$

and, since $\Delta y = 1$, $\Delta z = 1$,

$$= \frac{1}{2}\sigma\left(\frac{E_1}{k_x}\right)^2 \left[d(k_x^2 + k_z^2) + (k_z^2 - k_x^2)\frac{\sin 2k_x d}{2k_x}\right] \quad ,$$

where

$$\sigma = \omega\varepsilon'' \quad .$$

The attenuation can now be obtained from $\alpha = P_L/2P_T$ as

$$\alpha_z = \frac{\frac{1}{2}\omega\varepsilon''\left(\frac{E_1}{k_x}\right)^2\left[d\,(k_x^2 + k_z^2) + (k_z^2 - k_x^2)\frac{\sin 2k_x d}{2k_x}\right]}{\frac{1}{2}\omega\varepsilon\, k_z\, E_1^2\left[\frac{1}{k_x^2}\left(d + \frac{\sin 2k_x\, d}{2k_x}\right) + \frac{\sin^2 k_x\, d}{\varepsilon_r\, \alpha_x^3}\right]} .$$

Making use of normalized characteristic equations shown in the following section and of trigonometric identities involving sine and tangent, the above may be written in the form

$$\alpha_z = \frac{1}{2}\frac{\varepsilon_r''/\varepsilon_r'}{\sqrt{p^2 + 1}}\, k_o\, \frac{\varepsilon_r' p^2 qd'(1+\tan^2 qd') - p^2(\varepsilon_r' - 2p^2 - 2)\tan qd'}{p^2 qd'(1+\tan^2 qd') + (p^2 + \frac{q^2}{\varepsilon_r' p/q}\tan qd')\tan qd'} .$$

(1)

Attenuation Derived from the Characteristic Equations

There are three characteristic equations associated with the H-guide. Two of them result from evaluation of the wave equations in the dielectric and air regions, and the third is a consequence of field matching at the boundary.[1] The equations are

$$k_x^2 + k_y^2 + k_z^2 = k^2 \quad ,$$

$$-\alpha_x^2 + k_y^2 + k_z^2 = k_o^2 \quad ,$$

$$k_x \tan k_x d = \varepsilon_r \alpha_x \quad .$$

For the case of an infinite-width guide, the fields are constant in the y-direction ($k_y = 0$). Substituting this value in the above equations and normalizing gives

$$q^2 + (k_z/k_o)^2 = \varepsilon_r \quad , \qquad (2)$$

$$-p^2 + (k_z/k_o)^2 = 1 \quad , \qquad (3)$$

$$q \tan q\, d' = \varepsilon_r p \quad , \qquad (4)$$

and, after combining (2) and (3),

$$p^2 + q^2 + 1 = \varepsilon_r \quad , \qquad (5)$$

where

$$q = k_x/k_o \quad , \quad p = \alpha_x/k_o \quad , \quad d' = k_o d \quad .$$

In formulating the field equations the H-guide was assumed to have no losses. Hence, the field and medium constants k_x , k_y , k_z , ε_r were real numbers. In the presence of dielectric losses, however, these constants become complex. We write

$$k_z = k_z' - jk_z'' \quad ,$$

$$q = q' + jq'' \quad ,$$

$$p = p' + jp'' \quad ,$$

$$\varepsilon_r = \varepsilon_r' - j\varepsilon_r'' \quad .$$

It is noted that

$$k_z'' = \alpha_z \, .$$

Since the dielectric losses are low ($\varepsilon_r'' << \varepsilon_r'$), the resultant attenuation is assumed to be small also. This can be expressed by the following condition for the normalized values of the attenuation and phase constants,

$$k_z''/k_o << k_z'/k_o \quad .$$

Using the above two conditions in the complex characteristic equations and considering a practical range of operation, further approximations can be introduced,

$$p'' << p' \quad ,$$

$$q'' << q' \quad .$$

Substituting the complex constants in Eq. (5) and using the approximations, we obtain

$$\varepsilon_r' = q'^2 + p'^2 + 1 \quad ,$$

$$q'q'' = -\left(\frac{1}{2}\varepsilon_r'' + p'p''\right) \quad . \qquad (6)$$

Expanding Eq. (2) yields

$$k_z'/k_o = \varepsilon_r' - q'^2 \quad ,$$

$$k_z''/k_o = \frac{1}{2}\frac{\varepsilon_r'' + 2q'q''}{\sqrt{\varepsilon_r' - q'^2}} = \frac{1}{2}\frac{\varepsilon_r'' + 2q'q''}{k_z'/k_o} \quad .$$

Replacing $q'q''$ from Eq. (7) and k_z'/k_o from Eq. (3) gives

$$k_z''/k_o = -\frac{p'p''}{\sqrt{1+p'^2}} \quad . \qquad (7)$$

In order to find p'' in terms of the other constants, the remaining characteristic Eq. (4) must be used, where

$$(\varepsilon_r' - j\varepsilon_r'')(p' + jp'') = (q' + jq'')\tan(q' + jq'')d' \quad .$$

Expanding this equation and using the approximation $q''d' \ll 1$ enables us to write

$$\cosh q''d' \simeq 1 \quad ,$$

$$\sinh q''d' \simeq q''d' \quad .$$

Since $(\varepsilon_r''/\varepsilon_r')(p''/p') \ll 1$, we obtain

$$\varepsilon_r'p'[1+j(p''/p' - \varepsilon_r''/\varepsilon_r')] = (q'+jq'')\frac{\sinh q'd' + jq''d'\cos q'd'}{\cos q'd' - jq''d'\sin q'd'} \quad . \qquad (8)$$

This can be rationalized and separated into real and imaginary parts,

$$\varepsilon_r' p' = \frac{q' \tan q' d' - q''^2 d' (1 + \tan^2 q' d')}{1 + (q'' d' \tan q' d')^2} \quad , \qquad (9)$$

$$\varepsilon_r' p' (p''/p' - \varepsilon_r''/\varepsilon_r') = \frac{q'' \tan q' d' + q'' q' d' (1+\tan^2 q' d')}{1 + (q'' d' \tan q' d')^2} \quad , \qquad (10)$$

Combining the two equations yields

$$p''/p' - \varepsilon_r''/\varepsilon_r' = \frac{q'' \tan q' d' + q'' q' d' (1 + \tan^2 q' d')}{q' \tan q' d' - q''^2 d' (1 + \tan^2 q' d')}$$

The denominator of the right-hand side may be simplified if the following approximation is introduced,

$$q' \tan q' d' >> q''^2 d' (1 + \tan^2 q' d') \quad . \qquad (11)$$

We find then

$$p''/p' - \varepsilon_r''/\varepsilon_r' = \frac{q''}{q'} + q'' d' \left[\frac{1 + \tan^2 q' d'}{\tan q' d'} \right] . \qquad (12)$$

At the end of this section it is shown that Eq. (11) forms part of the condition for the agreement of the power and the characteristics method. After substituting q'' from Eq. (6) into Eq. (12) and solving for $p' p''$, Eq. (7) yields for k_z''/k_o

$$\frac{k_z''}{k_o} = \frac{1}{2} \frac{\varepsilon_r''/\varepsilon_r'}{\sqrt{1 + p'^2}} \frac{p'^2 \varepsilon_r' q' d' (1+\tan^2 q' d') - p'^2 (\varepsilon_r' - 2p'^2 - 2) \tan q' d'}{p'^2 q' d' (1+\tan^2 q' d') + (\varepsilon_r - 1) \tan q' d'} \quad . \qquad (13)$$

Comparison of Eqs. (13) and (1) shows that the two results are identical except for the second term in the denominator. In order for these two terms to be equal, the complex characteristic

equation $\varepsilon_r p = q \tan q d$ requires that

$$\varepsilon_r' p' = q' \tan q' d' \qquad (14)$$

and

$$\varepsilon_r' - 1 = p'^2 + \frac{q'^2}{\varepsilon_r' p'/q'} \tan q' d' \quad ,$$

which is equivalent to the second term in the denominator of Eq. (1). However, in order for Eq. (14) to be correct, the second terms of the numerator and denominator of Eq. (9) must be negligible compared to the first terms, respectively, i.e.

$$q' \tan q' d' >> q''^2 d' (1 + \tan^2 q' d')$$

and

$$1 >> (q'' d' \tan q' d')^2$$

These two conditions can be simplified and combined to give the following basic condition under which the two methods of computing the attenuation lead to practically identical results,

$$q'' d' << \tan q' d' << \frac{1}{q'' d'} \quad . \qquad (15)$$

An Alternate Method of Using the Characteristic Equations

In practice, ε_r' , ε_r'' , and d are known and the other quantities of the characteristic equation must be found in order to determine the attenuation. The two complex Eqs. (4) and (5) represent four equations and contain seven unknowns. Hence, known values of the above three constants should enable one to find a unique solution for the other four quantities. This approach requires solving a complex transcendental equation, a rather difficult task. The only way to avoid solving

a transcendental equation is to assume that the known factors are q' , q'' , and d. Obviously from the practical point of view q' and q'' are not known at first. However, once we have obtained the solution by choosing values for q, the results can be arranged such that the independent variables are ε_r' , ε_r'' , and d.

Consider first the equation

$$\varepsilon_r p = q \tan q d \quad ; \quad (\varepsilon_r' - j\varepsilon_r'')(p' + jp'') = A' + jA''$$

Since q' , q'' , and d are known, the right-hand side of the equation is a known complex number. Since $\varepsilon_r'' p''/\varepsilon_r' p'$ is small compared to 1, it can be neglected. Equating real and imaginary parts, we obtain

$$\varepsilon_r' p' = A' \quad , \tag{16}$$

$$\varepsilon_r' p' (p''/p' - \varepsilon_r''/\varepsilon_r') = A'' \quad ,$$

or

$$p''/p' - \varepsilon_r''/\varepsilon_r' = A''/A' \quad . \tag{17}$$

Combining Eqs. (16) and (6) gives the cubic equation

$$p'^3 + (q'^2 + 1) p' - A' = 0 \quad , \tag{18}$$

which may be solved using the computer. For a lossy dielectric, real positive values of p' are the only acceptable solutions. By substitution of ε_r'' from Eq. (6) into Eq. (17), a relation for the quantity $p' p''$ is found

$$p' p'' = \frac{A''/A - 2 q' q''/\varepsilon_r'}{1/p'^2 + 2/\varepsilon_r'} \tag{19}$$

which in turn is substituted into Eq. (7) to find the attenuation in terms of ε_r' , ε_r'' , q' , and q'' .

Figure 2.2 shows the normalized attenuation versus normalized values $d/\lambda o$ with ε_r' as parameter.

Conclusions

In order for the attenuation derived from power relationships to agree with that derived from the characteristic equations, certain restrictions apply. These restrictions may be expressed by

$$q'' d' << \tan q' d' << 1/q'' d' \quad .$$

These conditions have to be satisfied in addition to those which assure acceptable approximations for both computation methods individually, namely,

$$\varepsilon_r'' << \varepsilon_r' \ , \quad k_z'' << k_z \ , \quad p'' << p' \ , \text{ and } q'' << q' \quad .$$

Comparison of this inequality with Eq. (22) of Appendix I shows that it is the more stringent condition.

It is also assumed that derivation of the attenuation from the characteristic equations constitutes a more rigorous approach and hence gives a more accurate result. This should be expected since the computation of transmitted power and power loss are made from field equations valid for a lossless structure. While in solving for attenuation from the characteristic equations no assumption of zero-losses is made.

Appendix I

Consideration of a varying $q'd'$ shows that ε_r' or p' take negative values when $q'd'$ approaches $n\pi/2$ for $n = 1, 2, 3$ Such a condition would be unrealizable for a lossy structure.

To find the limitation imposed on the value of $q'd'$ as a result of the realizability condition, we write $q'd' = n\frac{\pi}{2} \pm \Delta\phi$, where $\Delta\phi << \pi/2$ 1 and substitute these quantities in Eq. (8). The number n may be an odd or even integer.

For odd n, we introduce $q'd' = n\pi/2 - \Delta\phi$. We find

$$\varepsilon_r'p'[1 + j(p''/p' - \varepsilon_r''/\varepsilon_r')] = (q' + jq'')$$

$$\frac{\sin(n\frac{\pi}{2} - \Delta\phi) + jq''d'\cos(n\frac{\pi}{2} - \Delta\phi)}{\cos(n\frac{\pi}{2} - \Delta\phi) - jq''d'\sin(n\frac{\pi}{2} - \Delta\phi)} \quad .$$

Since $\Delta\phi << \pi/2$, $\sin\Delta\phi \simeq \Delta\phi$, and $\cos\Delta\phi \simeq 1$, expanding the preceding equation and using these approximations gives

$$\varepsilon_r'p' = \frac{q'\Delta\phi - q''^2d'}{\Delta\phi^2 + (q''d')^2} \quad , \qquad (19)$$

$$p''/p' - \varepsilon_r''/\varepsilon_r' = \frac{q''\Delta\phi + q'q''d'}{\Delta\phi^2 + (q''d')^2}$$

From Eq. (19) we conclude, i.e. since $\varepsilon_r'p'$ must be positive, that $q'\Delta d - q''^2d' > 0$ or $\Delta\phi > q''^2d'/q'$.

Since $\tan q'd' = \tan(n\frac{\pi}{2} - \Delta\phi) = \cot\Delta\phi \simeq 1/\Delta\phi$, we find that

$$\tan q'd' < \frac{q'}{q''^2d'} \qquad (20)$$

must be satisfied.

For even n we write $q'd' = n\pi/2 + \Delta\phi$. Substituting it in Eq. (8) and expanding in a similar manner as above, we obtain

$$\varepsilon_r'p' = \frac{q'\Delta\phi - q''^2 d'}{\Delta\phi^2 + (q''d')^2}$$

$$p''/p' - \varepsilon_r''/\varepsilon_r' = \frac{q''\Delta\phi + q'q''d'}{\Delta\phi^2 + (q''d')^2}$$

Realizability requires $\Delta\phi > q''^2 d'/q'$, and, since $\tan g'd' = \tan(n\frac{\pi}{2} + \Delta\phi) = \tan\Delta\phi \simeq \Delta\phi$, we find the requirement that

$$\tan q'd' > \frac{q''^2 d'}{q'} \quad . \qquad (21)$$

Since $q'/q'' > 1$ and $q''/q' < 1$, the inequalities, Eq. (20) and Eq. (21) may be combined to give

$$q''d' < \tan q'd' < \frac{1}{q''d'} \quad . \qquad (22)$$

as a condition for realizable fields.

Appendix II

A set of graphs for the attenuation obtained from the result of the power method (Eq. 1) is presented in Fig. 2.3. The applicability of these are subject to the condition

$$q'' d' << \tan q' d' << 1/q'' d' \quad .$$

Thus, if the above condition holds for any range of values of H-guide operation, the curves in Fig. 2.3 may be used. They were checked by comparison of several points with values obtained by the characteristic equations. The checked points are indicated by arrows.

Furthermore, with a specified value for the field decrease, given by p' , the graphs in 2.3 may be used to determine the approximate value of the dielectric constant for which the attenuation is minimum. Using subsequently the curves in Figs. 2.2a and 2.2b, the thickness of the center slab can be found.

References

1 Collin, R. E., Foundation for Microwave Engineering, McGraw Hill Book Company, Sec. 3-8.

2 F. Jalali, F. J. Tischer, Field Decrease in H-Guides vs. Dielectric-Slab Parameters, Progress Report to NASA (June 15, 1969).

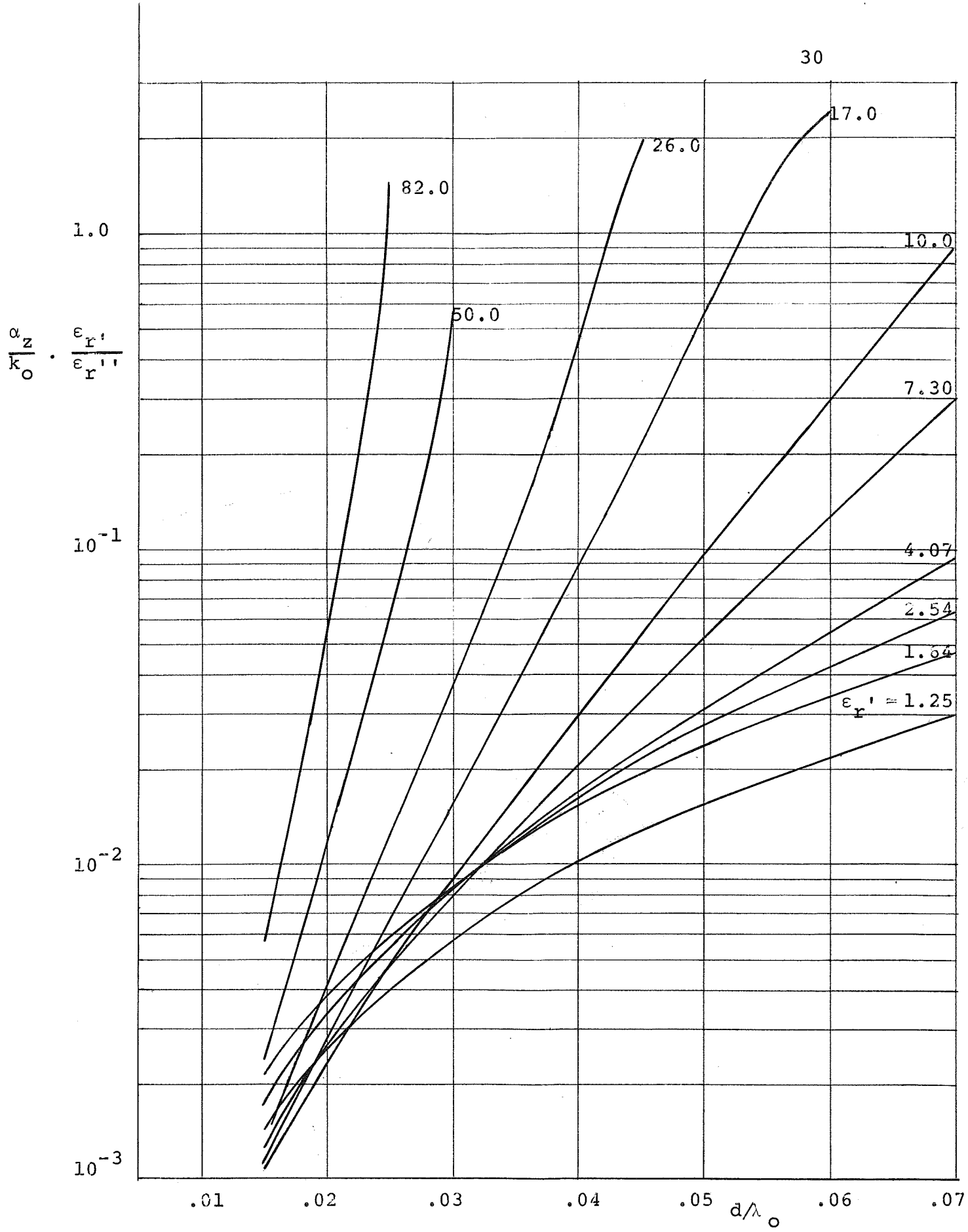

Fig. 2.2a Attenuation vs d/λ_o with ε_r' as parameter

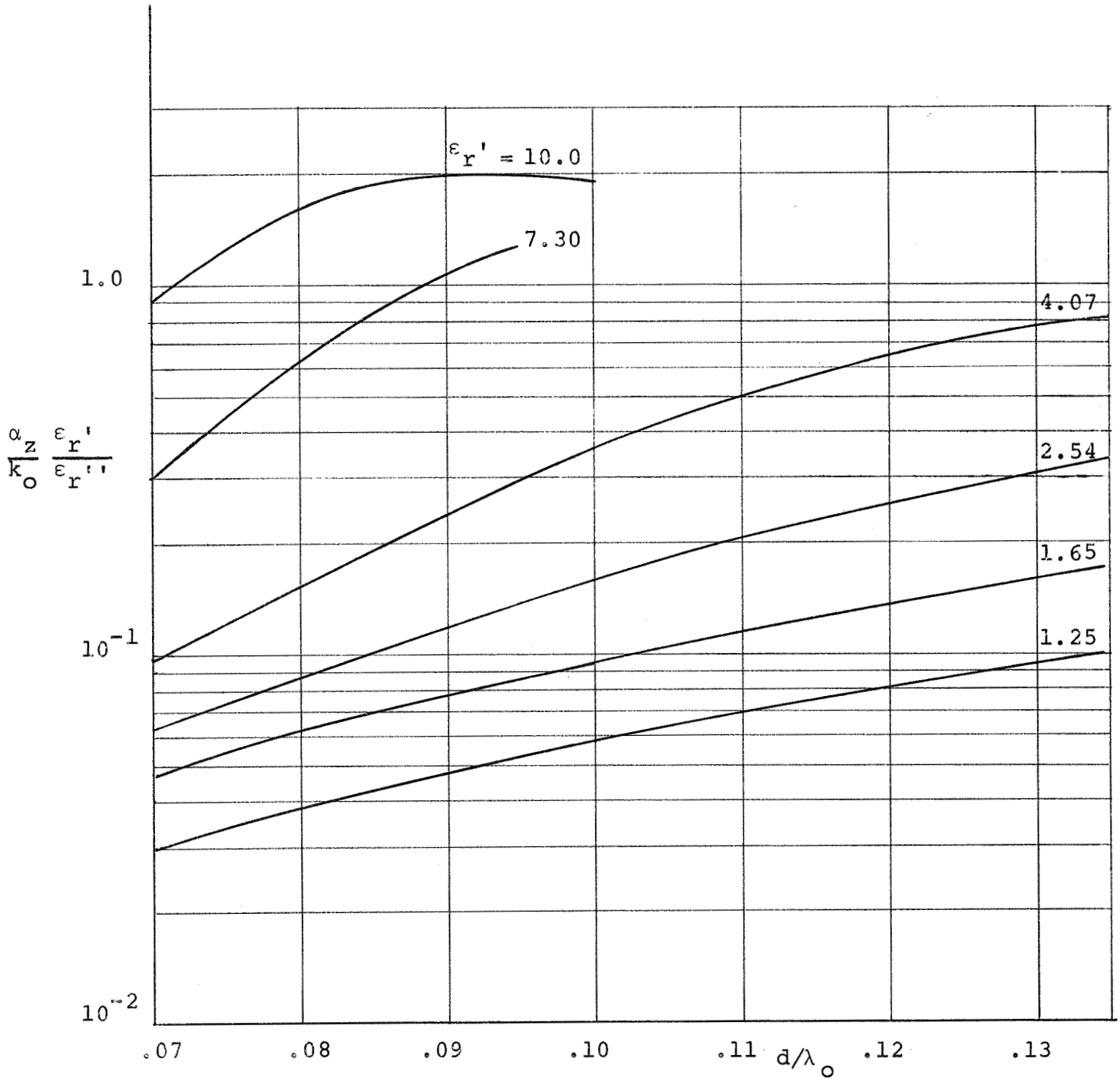

Fig. 2.2b Attenuation vs. d/λ_o with ε_r' as parameter

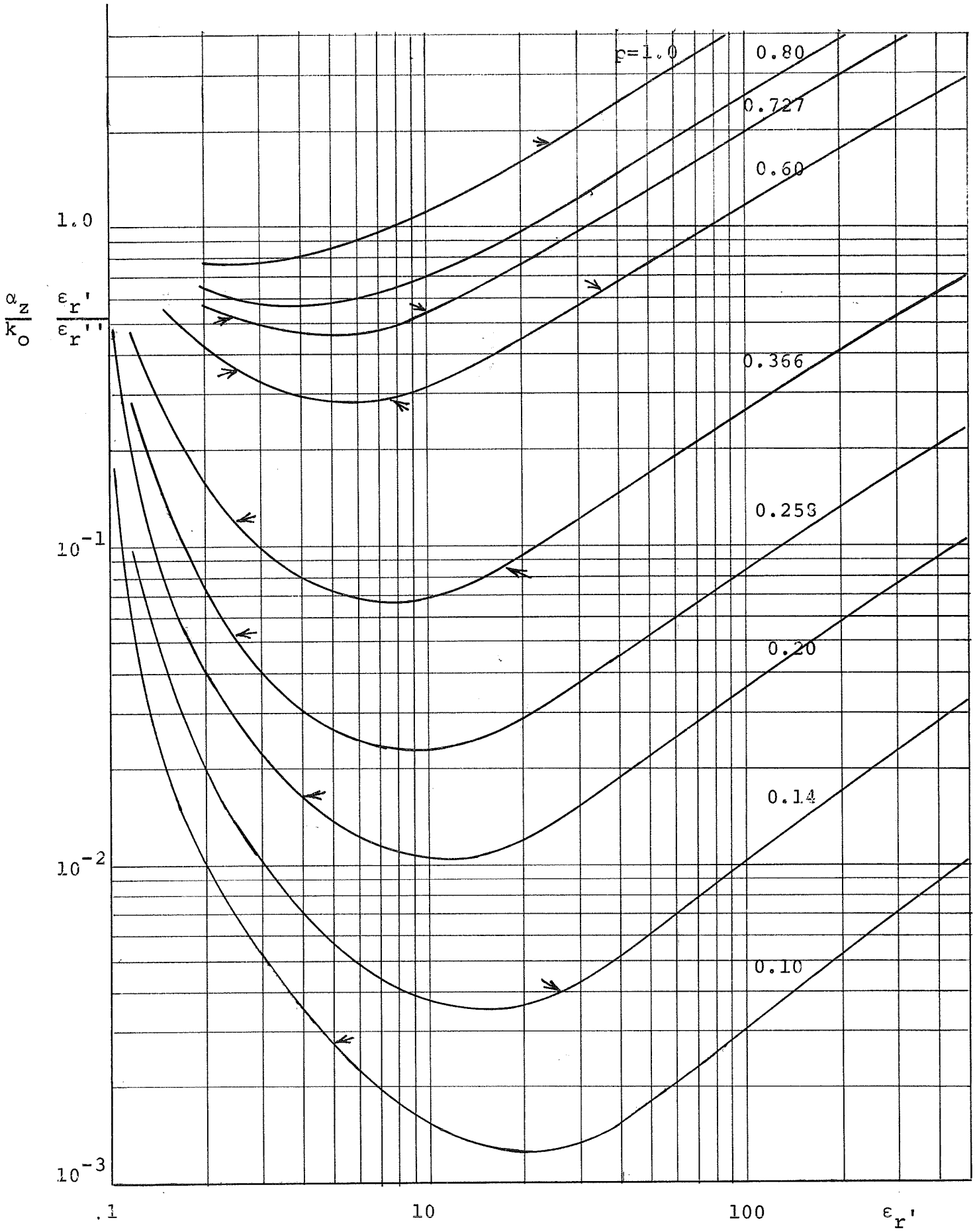

Fig. 2.3 Normalized attenuation vs. ε_r' with p as parameter ($p = \alpha_x/k_o$)

Part 3

CONFOCAL REFLECTOR GUIDE FOR MILLIMETER WAVES

Abstract

A beam waveguide is an attractive structure for the transmission of millimeter-wave signals in communications.

The present report continues the study of a parallel-reflector guide, where the millimeter wave energy is reflected between two cylindrical concave reflectors. The reflectors are spaced by their common radius of curvature. For the analysis of the beam reflector guide, a parallel-wall approach using Gaussian-Hermite functions is applied. The attenuation and loss characteristics of the guide, in particular the contribution by radiation, and the Q-value of a shorted section are considered.

CONFOCAL REFLECTOR GUIDE FOR MILLIMETER WAVES

Introduction

The paper deals primarily with the loss characteristics of confocal reflector guides and resonators, and it is an extension of a preceding report on this guide. A major part is concerned with the contribution to the attenuation by radiation with the computation based on considering the upper and lower openings as radiating surfaces. Since the loss characteristics of such a guide will be investigated experimentally later by the use of a shorted section of the guide as a resonator, the characteristics of such a resonator have been considered also to permit comparison of theoretical and experimental data.

As a first step the field distribution and the Q-value of a resonator composed of confocal circular-cylindrical reflector surfaces are computed. As a check of the correctness of the computed data, the results are compared with those obtained for a rectangular cavity. It is herewith assumed that for infinite radius of curvature, the confocal reflector resonator becomes a rectangular cavity.

The third part deals with the radiation losses of the open confocal reflector guide. The Kirchhoff-Huygens' principle is used for the determination of the fields resulting from radiation. From these fields, in turn, the Poyntings vector and the power losses per unit of length are computed. The final result is the attenuation due to radiation.

Confocal Resonator

The field distribution and the Q-value are computed for TE modes. Assume that the distribution function along the x-axis is given by a Gaussian-Hermite function.

$$E_o \exp(-\frac{x^2}{2a^2}) He_m(\frac{x}{a}) \quad .$$

The field in the resonator is then

$$E_x = E_o \exp(-\frac{x^2}{2a^2}) \; He_m(\frac{x}{a}) \; \sin k_y y \; \sin k_z z \quad .$$

Maxwell's equations in rectangular coordinates are

$$\frac{\partial E_z}{\partial y} - \frac{\partial E_y}{\partial z} = - j\omega\mu H_x \quad , \qquad \frac{\partial H_z}{\partial y} - \frac{\partial H_y}{\partial z} = + j\omega\varepsilon E_x \quad ,$$

$$\frac{\partial E_x}{\partial z} - \frac{\partial E_z}{\partial x} = - j\omega\mu H_y \quad , \qquad \frac{\partial H_x}{\partial z} - \frac{\partial H_z}{\partial x} = j\omega\varepsilon E_y \quad ,$$

$$\frac{\partial E_y}{\partial x} - \frac{\partial E_x}{\partial y} = - j\omega\mu H_z \quad , \qquad \frac{\partial H_y}{\partial x} - \frac{\partial H_x}{\partial y} = j\omega\varepsilon E_z \quad .$$

Since

$$E_y = E_z = 0 \quad , \quad k_o^2 = k_x^2 + k_y^2 + k_z^2 \quad , \quad k_y^2 = k_o^2 - k_z^2 \quad ,$$

we find

$$H_y = -\frac{1}{j\omega\mu} \frac{\partial E_x}{\partial z} = - \frac{k_z}{jk_o} \frac{1}{\eta} E_o \exp(-\frac{x^2}{2a^2}) \; He_m(\frac{x}{a}) \sin k_y y \; \cos k_z z \quad ,$$

$$H_z = \frac{1}{j\omega\mu} \frac{\partial E_x}{\partial y} = \frac{k_y}{jk_o\eta} E_o \exp(-\frac{x^2}{2a^2}) He_m(\frac{x}{a}) \cos k_y y \; \sin k_z z \quad ,$$

where

$$a = \sqrt{\frac{B}{k_y}} \quad , \quad \eta = \sqrt{\frac{\mu}{\varepsilon}} \quad , \quad k_o = \omega\sqrt{\mu\varepsilon} \quad , \text{ and } k_o\eta = \omega\mu \quad .$$

The field components are

$$E_x = E_o \exp(-\frac{x^2}{2a^2}) He_m(\frac{x}{a}) \sin k_y y \sin k_z z \quad ,$$

$$H_y = -\frac{k_z}{jk_o} \frac{E_o}{\eta} \exp(-\frac{x^2}{2a^2}) He_m(\frac{x}{a}) \sin k_y y \cos k_z z \quad ,$$

$$H_z = \frac{k_y}{jk_o\eta} E_o \exp(-\frac{x^2}{2a^2}) He_m(\frac{x}{a}) \cos k_y y \sin k_z z \quad .$$

The lowest-order-mode in the x-direction (m = 0) will be considered. The energy stored in a confocal resonator is given by

$$P_T = (U_E)max = \frac{\varepsilon}{2} \int_o^B \int_{-A/2}^{A/2} \int_o^C |E_x|^2 \, dz \, dx \, dy \quad ,$$

$$= \frac{\varepsilon}{2} \int_o^B 2 \int_o^{A/2} \int_o^C E_o^2 \exp(-\frac{x^2}{a^2}) \sin^2 k_y y \sin^2 k_z z \, dz dx dy \quad .$$

We introduce the error function

$$I = \int_o^{A/2} \exp(-\frac{x^2}{a^2}) \, dx \quad ,$$

set

$$t^2 = \frac{x^2}{a^2} \quad , \quad dx = a \, dt \quad ,$$

and for

$$\psi = \frac{A}{2} : \quad t = \frac{A}{2a} = \psi_o \quad ; \quad \psi_o = \frac{A}{2a} \quad \text{or} \quad \frac{A}{2\sqrt{\frac{B}{k_y}}} \quad .$$

The integral I becomes

$$I = a \int_o^{x_o} \exp(-t^2) \, dt \quad *$$

---

* Tables of higher functions (Jahnke-Emde). pp. 31

Die Fehlerfunktion $\Phi(x_o) = \frac{2}{\sqrt{\pi}} \int_o^{x_o} e^{-t^2} \, dt$

and we write using the error function $\Phi(x_o)$,

$$\frac{\sqrt{\pi}}{2}\,\Phi(x_o) = \frac{I}{a} \quad ,$$

or

$$I = \frac{a}{2}\sqrt{\pi}\;\Phi\;(x_o) \quad .$$

Substituting I into P_T , we obtain

$$P_T = \varepsilon\left[\frac{a}{2}\sqrt{\pi}\;\Phi(x_o)\right]\int_o^B \int_o^C E_o{}^2 \sin^2 k_y y\, \sin^2 k_z z\; dydz \quad .$$

The result is

$$P_T = \frac{\varepsilon E_o{}^2}{8}\; a\; B\; C\; \sqrt{\pi}\;\Phi\;(x_o) \quad .$$

The next term to be considered represents the current losses in the walls P_L . The conducting walls have a surface resistance R_s . The losses become

$$P_L = P_{L_1} + P_{L_2} + P_{L_3} \quad ,$$

$$P_L = \frac{R_s}{2}\left\{2\int_{-A/2}^{A/2}\int_0^C |H_z|^2_{y=0} dzdx + 2\int_o^B \int_{-A/2}^{A/2} |H_y|^2_{z=0}\; dxdy \right.$$

$$\left. + 2\int_o^B \int_o^C \left[|H_z|^2 + |H_y|^2\right]_{x=\frac{A}{2}} dz\; dy \right\} .$$

We substitute H_z and H_y into P_L and find

$$P_L = \frac{R_s}{2}\; 2\int_o^{A/2} 2\int_o^C \frac{k_z{}^2}{k_o{}^2}\,\frac{E_o{}^2}{\eta 2}\exp\left(-\frac{x^2}{a^2}\right)\sin^2 k_z z dzdx +$$

$$+ \frac{R_s}{2}\; 2\; 2\int_o^B \int_o^{A/2} \frac{k_z{}^2}{k_o{}^2}\,\frac{E_o{}^2}{\eta 2}\exp\left(-\frac{x^2}{a^2}\right)\sin^2 k_y y\; dx\; dy +$$

$$+ \frac{R_s}{2} \; 2 \int_o^B \int_o^C \frac{k_y^2}{k_o^2} \frac{E_o^2}{\eta 2} \exp(-\frac{A^2}{4a^2}) \cos^2 k_y y \; \sin^2 k_z z \; dzdy +$$

$$+ \frac{R_s}{2} \; 2 \int_o^B \int_o^C \frac{k_z^2}{k_o^2} \frac{E_o^2}{\eta 2} \exp(-\frac{A^2}{4a^2}) \sin^2 k_y y \; \cos^2 k_z z \; dzdy \quad .$$

Evaluation of the integrals gives

$$P_{L_1} = R_s \frac{k_y^2}{k_o^2 \eta^2} \; E_o^2 \; \frac{ac\sqrt{\pi}}{2} \; \Phi(x_o) \quad ,$$

$$P_{L_2} = R_s \frac{k_z^2}{k_o^2 \eta^2} \; E_o^2 \; \frac{aB\sqrt{\pi}}{2} \; \Phi(x_o) \quad ,$$

$$P_{L_3} = R_s \frac{E_o^2 B \; C}{4 k_o^2 \eta^2} \{\exp(-\frac{A^2}{4a^2})\} \; (k_y^2 + k_z^2) \quad .$$

If the path of the plane waves makes an angle ξ with the normal to side wall, one can write

$$k_y = k_o \cos\xi \quad , \quad k_z = k_o \sin\xi \quad ,$$

We introduce ξ in P_{L_1} , P_{L_2} , P_{L_3} ,

$$\psi_o = \frac{A}{2} \sqrt{\frac{k_y}{B}} = \frac{A}{2} \sqrt{\frac{k_o \cos\xi}{B}} \quad ,$$

$$P_{L_1} = \frac{R_s}{2} \frac{E_o^2}{\eta^2} \; C \sqrt{\frac{B\pi}{k_o \cos\xi}} \; \Phi(\frac{A}{2} \sqrt{\frac{k_o \cos\xi}{B}}) \; \cos^2\xi \quad .$$

Similarly P_{L_2} and P_{L_3} become

$$P_{L_2} = \frac{R_s}{2} \frac{E_o^2}{\eta^2} \; B \sqrt{\frac{B\pi}{k_o \cos\xi}} \; \Phi(\frac{A}{2} \sqrt{\frac{k_o \cos\xi}{B}}) \; \sin^2\xi \quad ,$$

$$P_{L_3} = \frac{R_s}{4} \frac{E_o^2}{\eta^2} \; B \; C \exp(-\frac{k_o A^2 \cos\xi}{4B}) \quad ,$$

since

$$\exp(-\frac{A^2}{4a^2}) = \exp(-\frac{k_o A^2 \cos\xi}{4B}) \quad ,$$

$$k_y^2 + k_z^2 = k_o^2(\cos^2\xi + \sin^2\xi) = k_o^2 \quad .$$

Similarly we express P_T in terms of the angle ξ ,

$$P_T = \frac{E_o^2 \; B \; C}{8} \sqrt{\frac{B\pi}{k_o \cos\xi}} \; \Phi(\frac{A}{2}\sqrt{\frac{k_o\cos\xi}{B}}) \quad .$$

The Q-value of a confocal resonator is defined by

$$Q = \frac{\omega_o P_T}{P_L} \quad .$$

The contributions by the various walls are

$$Q_1 = \frac{\omega_o P_T}{P_{L_1}} \quad , \quad Q_2 = \frac{\omega P_T}{P_{L_2}} \quad \text{and} \quad Q_3 = \frac{\omega_o P_T}{P_{L_3}} \quad .$$

Substituting the expressions found previously, we find

$$Q_1 = \frac{\omega_o P_T}{P_{L_1}} = \frac{\omega_o \varepsilon \eta^2 \; B}{4R_s \cos^2\xi} \quad ,$$

$$Q_2 = \frac{\omega_o P_T}{P_{L_2}} = \frac{\omega_o \varepsilon \eta^2 \; C}{4R_s \sin^2\xi} \quad ,$$

and

$$Q_3 = \frac{\omega_o \varepsilon \eta^2}{2R_s} \sqrt{\frac{B\pi}{k_o\cos\xi}} \; \frac{\Phi(\frac{A}{2}\sqrt{\frac{k_o\cos\xi}{B}})}{\exp(-\frac{k_o A^2 \cos\xi}{4B})} \quad .$$

The total Q of the confocal resonator is

$$\frac{1}{Q} = \frac{1}{Q_1} + \frac{1}{Q_2} + \frac{1}{Q_3} \quad .$$

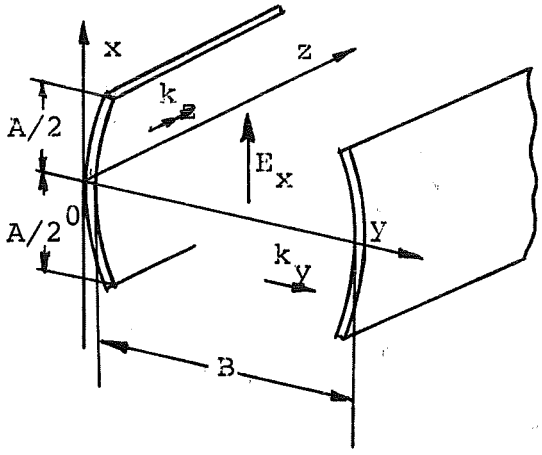

Fig. 3.1 Confocal Resonator

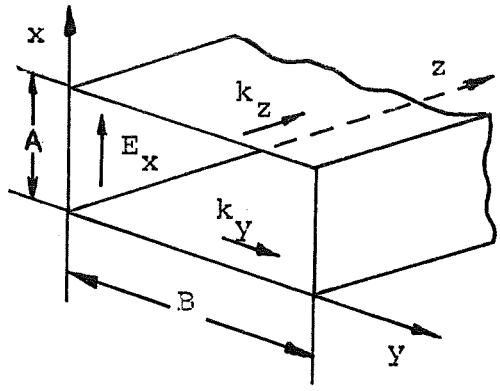

Fig. 3.2 Rectangular-cavity resonator

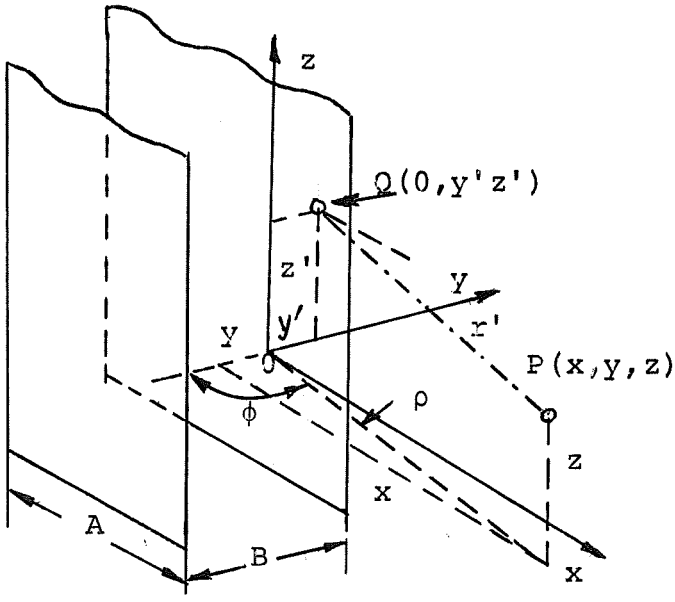

Fig. 3.3 Field intensity at observing point P

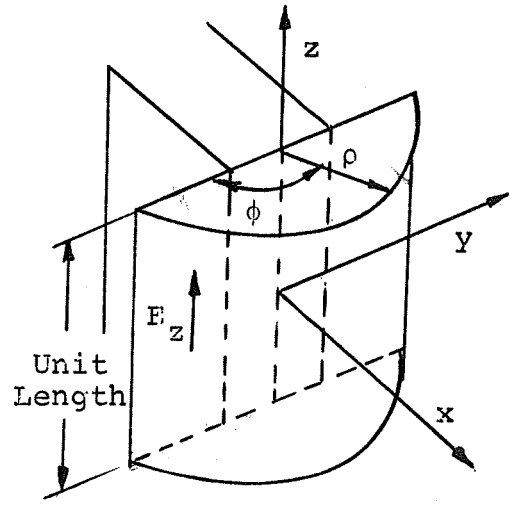

Fig. 3.4 The guide in a semi-circular cylinder

Substitution of the above results gives

$$\frac{1}{Q} = \frac{4R_s \cos^2\xi}{\omega_o \varepsilon \eta^2 B} + \frac{4R_s \sin^2\xi}{\omega_o \varepsilon \eta^2 C} + \frac{2R_s \exp\left(-\frac{k_o A^2 \cos\xi}{4B}\right)}{\varepsilon \omega_o \eta^2 \sqrt{\frac{B\pi}{k_o \cos\xi}}\, \Phi\left(\frac{A}{2}\sqrt{\frac{k_o \cos\xi}{2}}\right)} \quad .$$

Rectangular Cavity Resonator

For comparison, the Q-value is determined of a rectangular cavity resonator for TE modes. The fields are given by

$$E_x = E_o \sin k_y y \sin k_z z \quad ,$$

$$H_y = -\frac{k_z}{jk_o}\frac{E_o}{\eta} \sin k_y y \cos k_z z \quad ,$$

$$H_z = \frac{k_y}{jk_o}\frac{E_o}{\eta} \cos k_y y \sin k_z z \quad .$$

The energy stored in the resonator with dimension A, B, and C becomes

$$P_T = (U_E)_{max} = \frac{\varepsilon}{2} \int_o^B \int_o^A \int_o^C |E_x|^2 \, dzdxdy \quad ,$$

$$= \frac{\varepsilon}{8} A\, B\, C\, E_o^2 \quad .$$

The energy loss in the side walls is

$$P_{L_1} = \frac{R_s}{2}\, 2 \int_o^A \int_o^C |H_z|^2_{y=0} \, dzdx \quad ,$$

$$= \frac{R_s}{2}\, A\, C \left(\frac{k_y^2}{k_o^2}\frac{E_o^2}{\eta^2}\right) \quad ,$$

$$= \frac{R_s}{2}\frac{E_o^2}{\eta^2}\frac{k_y^2}{k_o^2}\, A\, C \quad .$$

It follows

$$Q_1 = \frac{\omega_o P_T}{P_{L_1}} = \frac{\omega_o \varepsilon B \eta^2 k_o^2}{4 R_s k_y^2} \quad .$$

If we substitute

$$k_y = k_o \cos\xi \quad ,$$

$$Q_1 = \frac{\omega_o \varepsilon}{4R_s} \frac{B\eta^2}{\cos^2\xi}$$

The energy loss due to front and back walls is

$$P_{L_2} = \frac{R_s}{2} \, 2 \int_o^A \int_o^B |H_y|^2_{z=0} \, dxdy \quad ,$$

or

$$P_{L_2} = \frac{R_s E_o^2}{2\eta^2} \, A \, B \sin^2\xi \quad .$$

Hence,

$$Q_2 = \frac{\omega_o \varepsilon \eta^2 \, C}{4 R_s \sin^2\xi} \quad .$$

The losses due to the top and floor are as follows:

$$P_{L_3} = \frac{R_s}{2} \, 2 \int_o^B \int_o^C [|H_z|^2 + |H_y|^2] \, dzdy$$

$$= \frac{R_s}{2} \, 2 \int_o^B \int_o^C \left(\frac{k_y^2}{k_o^2} \frac{E_o^2}{\eta^2} \cos^2 k_y y \sin^2 k_z z + \right.$$

$$\left. + \frac{k_z^2}{k_o^2} \frac{E_o^2}{\eta^2} \sin^2 k_y y \cos^2 k_z z \right) dzdy$$

$$= \frac{E_o^2}{\eta^2} \frac{B \, C \, R_s}{2} \quad ,$$

and

$$Q_3 = \frac{\omega_o P_T}{P_{L_3}} = \frac{\omega_o \varepsilon A}{4} \frac{\eta^2}{R_s} \quad .$$

The total Q of the rectangular resonator is given by

$$\frac{1}{Q} = \frac{1}{Q_1} + \frac{1}{Q_2} + \frac{1}{Q_3} \quad ,$$

$$= \frac{4R_s \cos^2\xi}{\omega_o \varepsilon B \eta^2} + \frac{4R_s \sin^2\xi}{\omega_o \varepsilon C \eta^2} + \frac{4R_s}{\omega_o \varepsilon A \eta^2} \quad ,$$

$$= \frac{4R_s}{\omega_o \varepsilon \eta^2} \left(\frac{\cos^2\xi}{B} + \frac{\sin^2\xi}{C} + \frac{1}{A}\right) \quad .$$

Confocal Reflector Guide

The field distribution is determined for the TE mode. We assume that E_x is defined by

$$E_x = E_o \exp\left(-\frac{x^2}{2a^2}\right) He_m\left(\frac{x}{a}\right) \sin k_y y \; e^{-jk_z z} \quad .$$

It is possible to solve for H_y and H_z in terms of E_x ,

$$\frac{\partial E_x}{\partial z} - \frac{\partial E_z}{\partial x} = -j\omega\mu H_y \quad .$$

Since $E_z = 0$, we find

$$H_y = \frac{k_z}{k_o \eta} E_o \exp\left(-\frac{x^2}{2a^2}\right) He_m\left(\frac{x}{a}\right) \sin k_y y \; e^{-jk_z z} \quad ,$$

where

$$\omega\mu = k_o \eta \quad .$$

Similarly, H_z can be found from

$$\frac{\partial E_y}{\partial x} - \frac{\partial E_x}{\partial y} = -j\omega\mu H_z \quad .$$

Since $E_y = 0$ and substituting E_x we obtain

$$-k_y E_o \exp(-\frac{x^2}{2a^2}) \; He_m(\frac{x}{a}) \; \cos k_y y \; e^{-jk_z z} = -j\omega\mu H_z$$

or

$$H_z = \frac{k_y}{jk_o\eta} E_o \exp(-\frac{x^2}{2a^2}) \; He_m(\frac{x}{a}) \; \cos k_y y \; e^{-jk_z z} \quad .$$

We calculate next the energy flowing into the confocal reflector m =0 :

$$P_T = \int_{-A/2}^{A/2} \int_o^B \frac{1}{2} (E_x H_y^*) \, dydx \quad ,$$

$$= \frac{k_z}{2k_o\eta} E_o^2 \frac{B}{2} \left[\int_{-A/2}^{A/2} \exp(\frac{x^2}{a^2}) \, dx \right] \quad .$$

Previously the error function was introduced,

$$I = \int_o^{A/2} \exp(-\frac{x^2}{a^2}) \, dx \quad .$$

The above equation can be expressed by the error function,

$$P_T = \frac{k_z}{2k_o\eta} E_o^2 \, B \, [I] \quad .$$

To obtain the power loss in the side walls, we introduce the surface resistance R_s and find for the losses

$$P_{L_1} = \frac{R_s}{2} \, 2 \int_{-A/2}^{A/2} \int_o^C |H_z|^2_{y=0} \, dzdx \quad ,$$

$$= \frac{R_s \, C \, k_y^2}{k_o^2 \eta^2} E_o^2 \, 2 \, [I] \quad .$$

Similarly, the power loss on the top and bottom surfaces is

$$P_{L_3} = \frac{R_s}{2}\, 2 \int_0^B \int_0^C \left[|H_z|^2 + |H_y|^2\right]_{x=\frac{A}{2}} dzdy \quad ,$$

$$= \frac{R_s E_o^2}{2\eta^2} \left(\frac{k_y^2 + k_z^2}{k_o^2}\right) \exp\left(-\frac{A^2}{4a^2}\right) \quad ,$$

$$= \frac{R_s E_o^2}{2\eta^2} \exp\left(-\frac{A^2}{4a^2}\right) \quad .$$

The attenuation loss of a confocal reflector guide is considered next. The contribution to the attenuation arising from sidewall losses is

$$\alpha_s = \frac{P_{L_1}}{2P_T}$$

$$= \frac{\frac{R_s\, C\, k_y^2}{k_o^2 \eta^2} E_o^2\, 2[I]}{2\, \frac{k_z}{2k_o\eta} E_o^2\, B\, [I]} = \frac{2R_s\, k_y^2}{k_o k_z \eta\, B} \quad ,$$

where C = unit length. The part of the attenuation due to losses in the top and bottom surfaces becomes

$$\alpha_T = \frac{P_{L_3}}{2P_T}$$

$$= \frac{\frac{R_s E_o^2}{2\eta^2} \exp\left(-\frac{A^2}{4a^2}\right)}{2\, \frac{k_z}{2k_o\eta} E_o^2\, [I]} = \frac{R_s\, k_o \exp\left(-\frac{A^2}{4a^2}\right)}{2k_z\, \eta\, [I]\, B} \; ; \; a = \sqrt{\frac{B}{k_y}} \quad .$$

If we set $a \to \infty$, then $\exp\left(-\frac{A^2}{4a^2}\right) \to 1$. The integral [I] becomes,

$$I = \lim_{a\to\infty} \int_0^{A/2} \exp\left(-\frac{x^2}{2a^2}\right) dx = \frac{A}{2} \quad .$$

Substituting these values into α_T , we obtain the corresponding part of the attenuation of the rectangular waveguide,

$$\alpha_T = \frac{R_s k_o}{k_z \eta A} \quad .$$

The total attenuation of the confocal reflector guide is

$$\alpha = \alpha_s + \alpha_T = \frac{2R_s k_y^2}{k_o k_z \eta B} + \frac{R_s k_o \exp(-\frac{A^2}{4a^2})}{2 k_z \eta [I] E} \quad ,$$

$$= \frac{R_s}{k_z \eta B} \left[\frac{2k_y^2}{k_o} + \frac{k_o \exp(-\frac{A^2}{4a^2})}{2[I]} \right] ,$$

and the total attenuation for $a \to \infty$ (rectangular guide) becomes

$$\alpha = \alpha_s + \alpha_T = \frac{2R_s k_y^2}{k_o k_z \eta B} + \frac{R_s k_o}{k_z \eta A} \quad ,$$

$$= \frac{R_s}{k_z \eta B} \left[\frac{2k_y^2}{k_o} + k_o \frac{1}{A} \right] \quad .$$

This result agrees with the equation obtained directly for the rectangular waveguide[1] and may be used as a check of the correctness of the above equation for the confocal guide closed on top and bottom by conducting walls.

Calculation of the Poynting Vectors Due to the Second and Third Order Field Distributions In the Top and Bottom Surfaces of the Confocal Reflector Guide

It was shown that the field distributions in the confocal waveguide are given by

$$E_x = E_o \exp(-\frac{x^2}{2a^2}) \, He_m(\frac{x}{a}) \, \sin k_y y \, e^{-jk_z z} \quad ,$$

$$H_y = \frac{k_z}{k_o \eta} E_o \exp\left(-\frac{x^2}{2a^2}\right) He_m\left(\frac{x}{a}\right) \sin k_y y \, e^{-jk_z z} \quad ,$$

$$H_z = \frac{k_y}{jk_o \eta} E_o \exp\left(-\frac{x^2}{2a^2}\right) He_m\left(\frac{x}{a}\right) \cos k_y y \, e^{-jk_z z} \quad .$$

The x-component of the Poynting vector is defined by

$$S_x = E_y H_z^* - E_z H_y^* \quad .$$

Since the above approximate equations have no components E_y and E_z, first-order perturbation terms are computed from Maxwell's equations. We start with E_x' , H_y' , and H_z' to obtain S_x' . Assuming that $H_x' \simeq 0$, the E_y' is obtained from Maxwell's equations as

$$E_y' = -\frac{1}{j\omega\varepsilon} \frac{\partial H_z}{\partial x} \quad ,$$

$$= \frac{k_y}{\omega \varepsilon k_o \eta} E_o \left(-\frac{x}{a^2}\right) \exp\left(-\frac{x^2}{2a^2}\right) \cos k_y y \, e^{-jk_z z} \quad .$$

We obtain for E_y' = (real term) $e^{-jk_z z}$. Similarly, we compute E_z' and find

$$E_z' = \frac{1}{j\omega\varepsilon} \frac{\partial H_y}{\partial x} \quad ,$$

$$= \frac{k_z}{j\omega\varepsilon k_o \eta} E_o \left(-\frac{x}{a^2}\right) \exp\left(-\frac{x^2}{2a^2}\right) \sin k_y y \, e^{-jk_z z} \quad ,$$

and write E_z' = (imaginary term)$e^{-jk_z z}$. Since the original equations for H_y and H_z can be written in similar form as

$$H_y = \text{(real term)} \, e^{-jk_z z} \quad ,$$

$$H_z = \text{(imaginary term)} \, e^{-jk_z z} \quad ,$$

one obtains $S_x' = E_y'$ (real). H_z (imaginary) - E_z' (imaginary). H_y (real). This shows that S_x' is imaginary and indicates a reactive power flow through the top and bottom surfaces. In a second attempt a second-order Poynting's vector is derived given by

$$S_x'' = E_y'' H_z''^* - E_z'' H_y''^* \quad .$$

We find the second-order field quantities as

$$H_x'' = -\frac{1}{j\omega\mu} \left[\frac{\partial E_z'}{\partial y} - \frac{\partial E_y'}{\partial x} \right] \quad ,$$

$$= \frac{k_y k_z E_o}{\mu \omega^2 k_o \eta} \left(-\frac{x}{a^2}\right) \exp\left(-\frac{x^2}{2a^2}\right) \cos k_y y \; e^{-jk_z z} -$$

$$- \frac{k_z k_y}{\omega^2 \mu^2 \varepsilon} E_o \left(-\frac{x}{a^2}\right) \exp\left(-\frac{x^2}{2a^2}\right) \cos k_y y \; e^{-jk_z z} \quad ,$$

which can be written as $H_x'' =$ (real term) $e^{-jk_z z}$. Similarly,

$$E_y'' = \frac{1}{j\omega\varepsilon} \left[\frac{\partial H_x''}{\partial z} - \frac{\partial H_z}{\partial x} \right] \quad ,$$

$$= - \frac{k_y k_z^2}{\omega^3 \mu \varepsilon^2 k_o \eta} E_o \left(-\frac{x}{a^2}\right) \exp\left(-\frac{x^2}{2a^2}\right) \cos k_y y \; e^{-jk_z z} +$$

$$+ \frac{k_z^2 k_y}{\omega^4 \mu^2 \varepsilon^2} E_o \left(-\frac{x}{a^2}\right) x \exp\left(-\frac{x^2}{2a^2}\right) \cos k_y y \; e^{-jk_z z} +$$

$$+ \frac{k_y}{\omega^2 \mu \varepsilon} \left(-\frac{x}{a^2}\right) E_o \exp\left(-\frac{x^2}{2a^2}\right) \cos k_y y \; e^{-jk_z z} \quad ,$$

hence

$$E_y'' = (\text{real term}) \cdot e^{-jk_z z} \quad .$$

Similarly one finds corresponding expressions for H_z'' , E_z'' , and H_y'' , which yield

$$H_z'' = (\text{imaginary})\ e^{-jk_z z} \quad ,$$

$$E_z'' = (\text{imaginary})\ e^{-jk_z z} \quad ,$$

and

$$H_y'' = (\text{real})\ e^{-jk_z z} \quad .$$

The second-order contribution S_x'' becomes then

$$S_x'' = E_y''\, H_z''^{*} - E_z''\, H_y''^{*} \quad ,$$

$$= E_y''(\text{real}).\ H_z''^{*}(\text{imaginary}) - E_z''(\text{imaginary}) H_y''^{*}(\text{real}) \quad ,$$

$$S_x'' = \text{imaginary} = \text{reactive} \quad .$$

This result indicates that under the assumed approximations radiation cannot be considered by determining the Poynting's vector in the upper and lower openings. Other methods have to be used to find the radiation losses.

Radiation Losses of the Confocal Reflector Guide

In this section Kirchhoff-Huygen's principle will be applied for the computation of radiation from the open surfaces of the reflector guide. The equations for the approximate field distributions in the guide are the same as at the beginning of the preceding section. The components of the field over the aperture of the reflector guide are

$$\tilde{E}_z = \frac{1}{j\omega\varepsilon} \frac{\partial H_y}{\partial x} \quad ,$$

$$= \frac{1}{j\omega\varepsilon} \left[\frac{k_z}{k_o \eta}\ E_o \left(\exp\left(-\frac{x'^2}{2a^2}\right)\right)\left(-\frac{x'}{a^2}\right) \cos k_y y'\ e^{-jk_z z}\right] \quad .$$

The component of the field at a source point is hence

$$\tilde{E}_z = \frac{k_z}{jk_o^2} E_o\left(-\frac{x'}{a^2}\right) \exp\left(-\frac{x'^2}{2a^2}\right) \cos k_y y' e^{-jk_z z'} ,$$

$$\tilde{H}_y = \frac{k_z}{k_o \eta} E_o \exp\left(-\frac{x'^2}{2a^2}\right) \cos k_y y' e^{-jk_z z'} .$$

The retarded Hertz vector can be written as

$$\Pi_e = \frac{1}{4\pi j\omega\varepsilon} \int_{s'} \frac{(n \times \tilde{H})}{r'} e^{-jk_o r'} ds' ,$$

$$\Pi_m = \frac{1}{4\pi j\omega\mu} \int_{s'} \frac{(n \times \tilde{E})}{r'} e^{-jk_o r'} ds' .$$

Substitution of H_y in Π_e and for $x' = \frac{A}{2}$ yields

$$\Pi_{ez} = \frac{1}{4\pi j\omega\varepsilon} \int_{s'} \frac{k_z}{k_o \eta} E_o \exp\left(-\frac{A^2}{8a^2}\right) \frac{\cos k_y y' e^{-jk_z z'} e^{-jk_o r'}}{r'} ds' ,$$

$$= \frac{E_o k_z}{4\pi j k_o^2} \exp\left(-\frac{A^2}{8a^2}\right) \int_{-B/2}^{B/2} \int_{-\infty}^{\infty} \frac{\cos k_y y' e^{-j(k_z z' + k_o r')}}{r'} dy' dz' .$$

Since

$$r' = \sqrt{\rho'^2 + (z - z')^2} ,$$

we write

$$\Pi_{ez} = \frac{E_o k_z}{4\pi j k_o^2} \exp\left(-\frac{A^2}{8a^2}\right) [I'] ,$$

where

$$I' = \int_{-B/2}^{B/2} \int_{\infty}^{\infty} \frac{\cos k_y y' e^{-j(k_z z' + k_o r')}}{\sqrt{\rho'^2 + (z - z')^2}} dy' dz' .$$

As a first step, we integrate with respect to z' . We introduce a new variable,

$$z' - z = \rho' \sinh t \ ,$$

and

$$\rho'^2 + (z - z')^2 = \rho'^2 + \rho'^2 \sinh^2 t = \rho'^2 \cosh^2 t \quad .$$

After substitution into I' , the integral becomes

$$I' = \int_{-B/2}^{B/2} \cos k_y y' \, dy' \, [I_o] \quad ,$$

where

$$I_o = \int_{-\infty}^{\infty} \exp[-j\rho' \{k_o \cosh t + k_z z + k_z \rho' \sinh t\}] \, dt \quad ,$$

$$= e^{-jk_z z} \int_{-\infty}^{\infty} \exp[-j\rho' (k_o \cosh t + k_z \sinh t)] \, dt \quad .$$

We assume next that $k_o^2 - k_z^2 = k_r^2$. The integral $[I_o]$ becomes then a Hankel function of zero order. The result is

$$I_o = -j\pi H_o^{(2)} (k_r \rho') \, e^{-jk_z z} \quad .$$

The asymptotic expansion of the Hankel function for large argument can be used for the computation of the radiation losses,

$$I_o \simeq -j\pi e^{-jk_z z} \sqrt{\frac{2}{\pi \rho' k_r}} \, e^{-j(k_r \rho' - \frac{\pi}{4})} \quad .$$

We can make the approximation $\rho' \simeq \rho + y' \cos\phi$, $\rho' \simeq \rho$ and find

$$I_o \simeq -j\pi e^{-jk_z z} \sqrt{\frac{2}{\pi \rho k_r}} \, e^{-j(k_r \rho + k_r y' \cos\phi - \frac{\pi}{4})} \quad ,$$

$$I_o = -j\pi H_o^{(2)}(k_r\rho)\, e^{-j(k_r y' \cos\phi)}\, e^{-jk_z z} \quad .$$

Hence, Π_{ez} becomes

$$\Pi_{ez} = \frac{-E_o k_z}{4k_o^2} \exp\left(-\frac{A^2}{8a^2}\right) H_o^{(2)}(k_r\rho)\, e^{-jk_z z} \int_{-B/2}^{B/2} \frac{e^{jk_y y} + e^{-jk_y y}}{2}\, e^{-jk_r y' \cos\phi}\, dy' \quad .$$

The integral is

$$\int_{-B/2}^{B/2} \frac{1}{2}\left[e^{j(k_y - k_r\cos\phi)y'} + e^{-j(k_y - k_r\cos\phi)y'}\right] dy' =$$

$$= \frac{1}{k_y^2 - k_r^2\cos^2\phi}\left[(k_y + k_r\cos\phi)\sin\left\{\frac{B}{2}(k_y - k_r\cos\phi)\right\} + \right.$$

$$\left. + (k_y - k_r\cos\phi)\sin\left\{\frac{B}{2}(k_y + k_r\cos\phi)\right\}\right] \quad .$$

Transformation of the result gives

$$= \frac{2}{k_y^2 - k_r^2\cos^2\phi}\left[k_y \sin\left(\frac{Bk_y}{2}\right)\cos\left(\frac{k_r B}{2}\cos\phi\right) - \right.$$

$$\left. - k_r \cos\left(\frac{Bk_y}{2}\right)\sin\left(\frac{k_r B}{2}\cos\phi\right)\right] \quad .$$

The field component

$$E_x = E_o \exp\left(-\frac{x^2}{2a^2}\right)\cos k_y y\, e^{-jk_z z} \quad ,$$

satisfies the boundary conditions

$$y = \frac{B}{2} \; : \quad \cos k_y y \Big|_{y = \frac{B}{2}} = 0 \quad \text{and} \quad \sin k_y y \Big|_{y = \frac{B}{2}} = 1 \quad .$$

Taking account of these conditions, the integral becomes finally

$$\int_{-B/2}^{B/2} \cos k_y y' \, e^{-jk_r y' \cos\phi} \, dy' = \frac{2 \cos\left(\frac{k_r B}{2} \cos\phi\right)}{k_y\left(1 - \frac{k_r^2}{k_y^2}\cos^2\phi\right)} \quad .$$

Substituting this result into Π_{ez}, we find

$$\Pi_{ez} = -\frac{E_o k_z}{2k_o^2 k_y} \exp\left(-\frac{A^2}{8a^2}\right) H_o^{(2)}(k_r\rho) e^{-jk_z z} \frac{\cos\left(\frac{k_r B}{2}\cos\phi\right)}{1 - \frac{k_r^2}{k_y^2}\cos^2\phi} \quad ,$$

since

$$k_r^2 \simeq k_o^2 - k_x^2 = k_y^2$$

and

$$k_y B = \left(n - \tfrac{1}{2}\right)\pi \quad ,$$

where n is odd. The final result is

$$\Pi_{ez} = -\frac{E_o k_z}{2k_o^2 k_y} \exp\left(-\frac{A^2}{8a^2}\right) H_o^{(2)}(k_y\rho) e^{-jk_z z} \frac{\cos\left[\left(n-\frac{1}{2}\right)\pi\cos\phi\right]}{\sin^2\phi} \quad .$$

Similarly we compute Π_m from the equation

$$\Pi_m = \frac{1}{4\pi j\omega\mu} \int_s' \frac{(n \times \tilde{E})}{r'} e^{-jk_o r'} \, ds' \quad ,$$

$$\Pi_{my} = \frac{1}{4\pi j\omega\mu} \int_s' \frac{k_z E_o}{jk_o^2}\left(-\frac{A}{2a^2}\right)\exp\left(-\frac{A^2}{8a^2}\right) \frac{\cos k_y y' \, e^{-jk_z z} e^{-jk_o r'}}{r'} ds' \quad ,$$

$$\Pi_{my} = -\frac{jE_o k_z}{4k_o^3\eta}\left(\frac{A}{2a^2}\right)\exp\left(-\frac{A^2}{8a^2}\right) H_o^{(2)}(k_y\rho) e^{-jk_z z} \frac{\cos\left[\left(n-\frac{1}{2}\right)\pi\cos\phi\right]}{\sin^2\phi} \quad .$$

We determine next the far-fields from the vector potentials according to

$$E_z = \nabla\,\nabla\cdot\Pi_{ez} + k_o^2\,\Pi_{ez} - j\omega\mu\left[\frac{\partial\Pi_{m\phi}}{\partial\rho} + \Pi_{m\phi}\,\frac{1}{\rho} - \frac{1}{\rho}\,\frac{\partial\Pi_{m\rho}}{\partial\phi}\right] \quad ,$$

and

$$E_\phi = \frac{\partial\Pi_{m\rho}}{\partial z} - \frac{ik_z}{\rho}\,\frac{\partial\Pi_{ez}}{\partial\rho} \quad ,$$

since

$$\nabla \times \Pi = \vec{a}_\rho\left[\frac{1}{\rho}\,\frac{\partial\Pi_z}{\partial\phi} - \frac{\partial\Pi_\phi}{\partial z}\right] + \vec{a}_\phi\left[\frac{\partial\Pi_\rho}{\partial z} - \frac{\partial\Pi_z}{\partial\rho}\right] + \vec{a}_z\left[\frac{1}{\rho}\,\frac{\partial(\rho\Pi_\phi)}{\partial\rho} - \frac{1}{\rho}\,\frac{\partial\Pi_\rho}{\partial\phi}\right] \quad .$$

Since the radiation amplitude decreases with $\rho^{-1/2}$, we may neglect the last term of E_z and E_ϕ. We use the identity

$$\nabla\nabla\cdot\Pi_{ez} + k_o^2\,\Pi_{ez} = (-k_z^2 + k_o^2)\,\Pi_{ez} = k_y^2\,\Pi_{ez} \quad ,$$

and the relationships

$$\Pi_{m\rho} = \Pi_{my}\cos(\pi-\phi) = -\,\Pi_{my}\cos\phi \;;\quad \Pi_{m\phi} = \Pi_{my}\sin\phi \quad .$$

Substituting these terms into E_z and E_ϕ, we obtain

$$E_z = k_y^2\,\Pi_{ez} - j\omega\mu\,\frac{\partial\Pi_{my}}{\partial\rho}\sin\phi \quad ,$$

and

$$E_\phi = -\,\frac{\partial\Pi_{my}}{\partial z}\cos\phi \quad .$$

After inserting Π_{my} and Π_{ez} we obtain finally

$$E_z = -\,\frac{E_o k_z e^{-jk_z z}}{2k_o^2}\exp\left(-\frac{A^2}{8a^2}\right)\left[k_y\,H_o^{(2)}(k_y\rho) + \right.$$

$$\left. + \frac{1}{k_y\eta}\left(\frac{A}{2a^2}\right)\frac{\partial H_o^{(2)}(k_y\rho)}{\partial\rho}\sin\phi\right]\frac{\cos\left[\left(n-\frac{1}{2}\right)\pi\cos\phi\right]}{\sin^2\phi} \quad .$$

Similarly,

$$E_\phi = (-jk_z)\ \frac{(-j)E_o k_z}{2k_o^3 k_y \eta}\ \left(\frac{A}{2a^2}\right)\exp\left(-\frac{A^2}{8a^2}\right)\ H_o^{(2)}(k_y\rho)$$

$$e^{-jk_z z}\ \frac{\cos\left[\left(n-\frac{1}{2}\right)\pi\cos\phi\right]}{\sin^2\phi}\ \cos\phi \quad .$$

These equations can be written as

$$E_z = -\frac{E_o k_z}{2k_o^2}\ \exp\left(-\frac{A^2}{8a^2}\right)\ e^{-jk_z z}\ F_z(\phi) \quad ,$$

$$E_\phi = -\frac{E_o k_z^2}{2k_o^3 k_y \eta}\ \left(\frac{A}{2a^2}\right)\ \exp\ \left(-\frac{A^2}{8a^2}\right)\ e^{-jk_z z}\ F_\phi(\phi) \quad ,$$

where

$$F_z(\phi) = \left[k_y\ H_o^{(2)}(k_y\rho) + \frac{1}{k_y\eta}\left(\frac{A}{2a^2}\right)\frac{\partial H_o^{(2)}(k_y\rho)}{\partial\rho}\ \sin\phi\right]$$

$$\frac{\cos\left[\left(n-\frac{1}{2}\right)\pi\cos\phi\right]}{\sin^2\phi} \quad ,$$

$$F_\phi(\phi) = \frac{\cos\left[\left(n-\frac{1}{2}\right)\pi\cos\phi\right]}{\sin^2\phi}\ \cos\phi \quad .$$

For the calculation of the radiation loss from the waveguide, we enclose the guide in a semi-circular cylinder of radius ρ and calculate the power flowing out the cylinder,

$$P_L = K_1^2 \int_o^\pi |F_z(\phi)|^2 \rho d\phi + K_2 \int_o^\pi |F_\phi(\phi)|^2 \rho d\phi \quad ,$$

where

$$K_1 = \frac{E_o k_z}{2k_o^2}\ \exp\ \left(-\frac{A^2}{8a^2}\right) \quad ,$$

$$K_2 = \frac{E_o k_z^2}{2k_o^3 k_y \eta} \left(\frac{A}{2a^2}\right) \exp\left(-\frac{A^2}{8a^2}\right) \quad ,$$

and

$$F_z(\phi) = [k_y H_o^{(2)}(k_y\rho) + \frac{1}{k_y\eta}\left(\frac{A}{2a^2}\right) \frac{\partial H_o^{(2)}(k_y\rho)}{\partial\rho} \sin\phi] \frac{\cos[(n-\frac{1}{2})\pi\cos\phi]}{\sin^2\phi} \quad ,$$

$$F_\phi(\phi) = \frac{\cos[(n-\frac{1}{2})\pi\cos\phi]}{\sin^2\phi} \cos\phi \quad .$$

The integrals of $F_z(\phi)$ and $F_\phi(\phi)$ will be

$$\int_o^\pi |F_z(\phi)|^2 \rho d\phi = \int_o^\pi [k_y H_o^{(2)}(k_y\rho)]^2 \frac{\cos^2[(n-\frac{1}{2})\pi\cos\phi]}{\sin^4\phi} \rho d\phi +$$

$$+ 2 [H_o^{(2)}(k_y\rho) \frac{A}{\eta 2a^2} \frac{\partial H_o^{(2)}(k_y\rho)}{\partial\rho}]$$

$$x \int_o^\pi \frac{\cos^2[(n-\frac{1}{2})\pi\cos\phi]}{\sin^4\phi} \sin\phi\rho d\phi +$$

$$+ \{\frac{1}{k_y\eta}\left(\frac{A}{2a^2}\right) \frac{\partial H_o^{(2)}(k_y\rho)}{\partial\rho}\}^2 x \int_o^\pi \sin^2\phi \; x$$

$$x \frac{\cos^2[(n-\frac{1}{2})\pi\cos\phi]}{\sin^4\phi} \rho d\phi \quad ,$$

$$\int_o^\pi |F_\phi(\phi)|^2 \rho d\phi = \int_o^\pi \frac{\cos^2[(n-\frac{1}{2})\pi\cos\phi]}{\sin^4\phi} \rho d\phi \quad .$$

The average power transported along the guide is

$$P_T = \int_{-A/2}^{A/2} \int_{o}^{B} \frac{1}{2} (E_x H_y^*) \, dydx \quad ,$$

$$= \frac{k_z E_o^2 B[I]}{2k_o \eta} \quad ,$$

where

$$[I] = \int_{o}^{A/2} \exp(-\frac{x^2}{a^2}) \, dx \quad .$$

If we neglect the field resulting from E_z, since it is much smaller than that caused by H_y, we write as an approximation

$$\int_{o}^{\pi} |F_z(\phi)|^2 \rho d\phi \simeq \int_{o}^{\pi} k_y^2 [H_o^{(2)}(k_y\rho)]^2 \frac{\cos^2[(n-\frac{1}{2})\pi\cos\phi]}{\sin^4\phi} \rho d\phi \, .$$

The asymptotic expansion of $H_o^{(2)}(k_y\rho)$ for a large argument is

$$H_o^{(2)}(k_y\rho) \simeq \sqrt{\frac{2}{\pi k_y \rho}} \, e^{-j(k_y\rho - \frac{\pi}{4})} \quad .$$

Substitution into $F_z(\phi)$ gives

$$\int_{o}^{\pi} |F_z(\phi)|^2 \rho d\phi \simeq \int_{o}^{\pi} k_y^2 \frac{2}{\pi k_y \rho} \frac{\cos^2[(n-\frac{1}{2})\pi\cos\phi]}{\sin^4\phi} \rho d\phi \quad ,$$

$$= \frac{2k_y}{\pi} [J] \quad ,$$

where

$$[J] = \int_{o}^{\pi} \frac{\cos^2[(n-\frac{1}{2})\pi\cos\phi]}{\sin^4\phi} \, d\phi \quad .$$

Hence,

$$P_L = K_1^2 \int_{o}^{\pi} |F_z(\phi)|^2 \rho d\phi \quad ,$$

$$P_L = \frac{E_o^2 k_z^2 k_y}{2k_o^2 \pi} \exp(-\frac{A^2}{4a^2}) \quad [J] \quad .$$

Since the radiated power is

$$P_L' = \frac{1}{2} \frac{|F_z(\phi)|^2}{\eta} \quad ,$$

the attenuation due to radiation from the upper and lower openings become

$$\alpha_R = \frac{P_L'}{2P_T} = \frac{\frac{E_o^2 k_z^2 k_y}{4k_o^2 \eta \pi} \exp(-\frac{A^2}{4a^2}) \quad [J]}{\frac{k_z E_o^2 B[I]}{2k_o \eta}} \quad ,$$

or

$$\alpha_R = \frac{k_y k_z [J]}{2\pi k_o B(I)} \exp(-\frac{A^2}{4a^2}) \quad ,$$

where

$$[I] = \int_o^{A/2} \exp(-\frac{x^2}{a^2}) \, dx \quad ,$$

and

$$[J] = \int_o^{\pi} \frac{\cos^2[(n-\frac{1}{2})\pi\cos\phi]}{\sin^4\phi} \, d\phi \quad .$$

Graphical evaluation of these results is shown in the following diagrams of Figs. 3.5 to 3.7.

References

1 J. D. Jackson, Classical Electrodynamics, John Wiley & Sons, Inc., New York, N. Y. (1962).

2 F. J. Tischer, Properties of the H-Guide at Microwaves and in the Millimeter-Wave Region, Proc. IEE(London), Vol. 106B, Suppl. 13, pp. 47-53 (January 1959).

3 T. Nakahara, Guided Beam Waves Between Parallel Concave Reflectors, IEEE Transactions on Microwave Theory and Technique, Vol. MTT-15, pp. 66-71 (February 1967).

4 G. D. Boyd, Confocal Multimode Resonator for MM Through Optical Wavelengths Masers, Bell Syst. Tech. J., pp. 489-507 (March 1961).

5 K. Takiyama, Radiation Characteristics of a Leaky H-Guide, Electronics and Communications in Japan, Vol. 50, pp. 1-9, (February 1967).

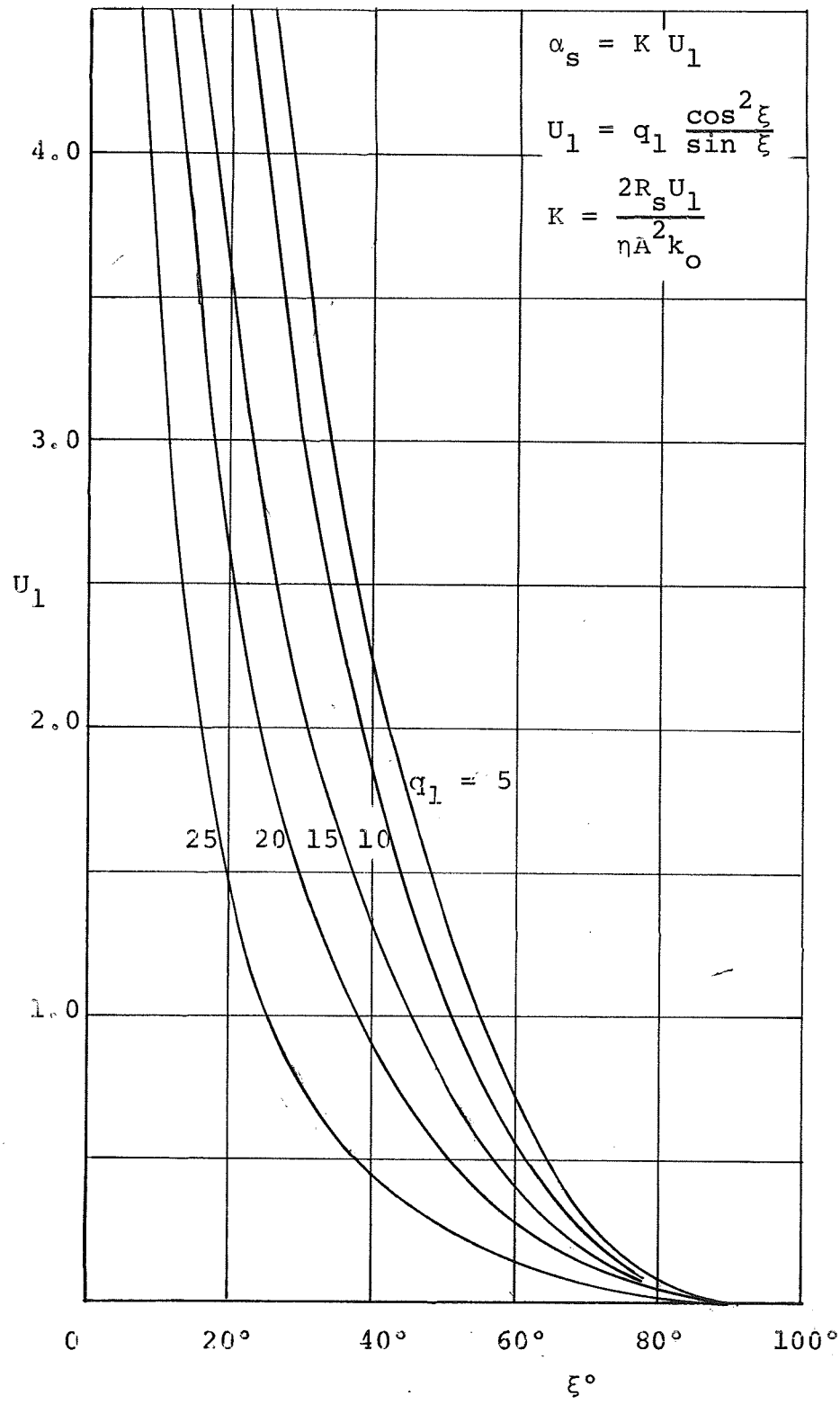

Fig. 3.5 Normalized attenuation constant α_s (side wall). Function U_1 vs. ξ .

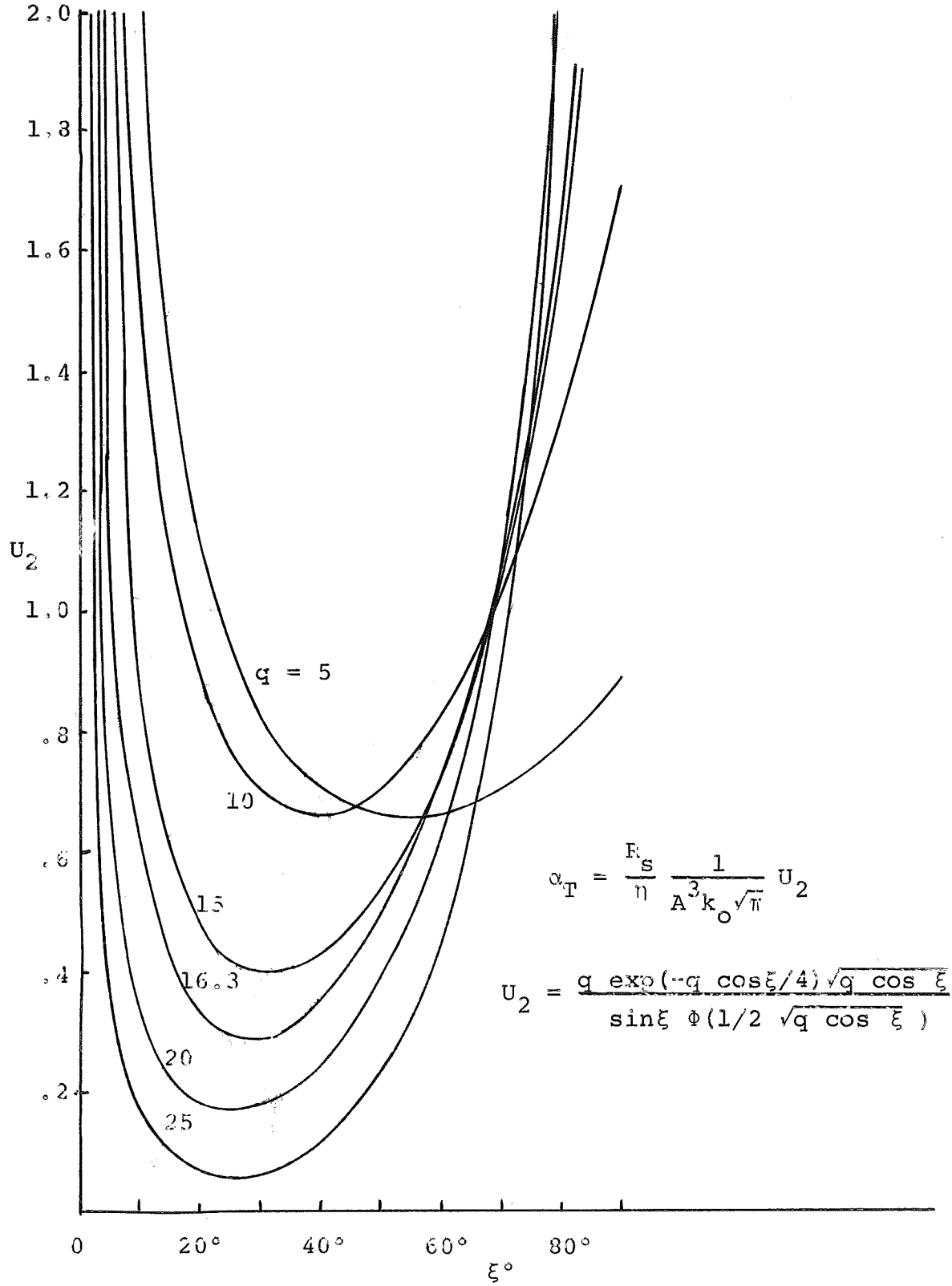

Fig. 3.6 Attenuation constant α_T .
Function U_2 vs. ξ and q .

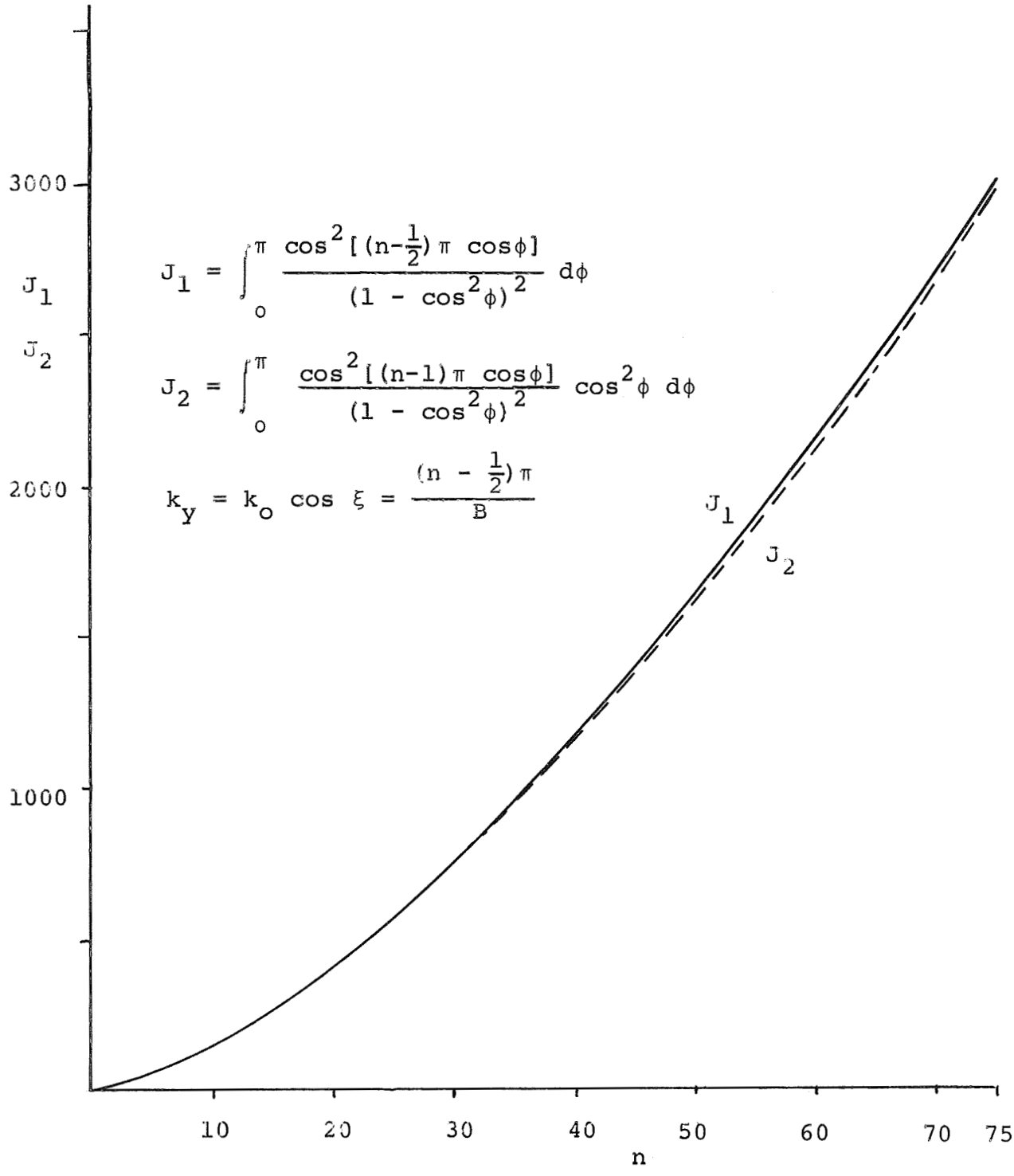

Fig. 3.7 Integrals J_1 and J_2 vs. n.

Part 4

STUDY OF THE EFFECTS OF SURFACE ROUGHNESS

Abstract

An outline of a study of the effects of surface roughness on the loss characteristics of waveguides, particularly the H-guide and the beam waveguide, is presented. The problem is very important at millimeter waves since the measured values of the attenuation are usually twenty to fifty per cent above the values predicted theoretically at present.

STUDY OF THE EFFECTS OF SURFACE ROUGHNESS

Introduction

Q-value measurements on resonant shorted sections of waveguides are used in this laboratory to determine the attenuation of non-conventional waveguides at millimeter waves. It is known that, in this frequency range, measured Q-values usually are between 60% and 80% of the theoretical values. At this time the sources of this discrepancy are not well understood. The wall losses are primarily a function of the surface resistance and this, in turn, of the conductor properties. At wavelengths longer than a few centimeters, surface resistance is determined by the bulk properties of the metal, but at wavelengths of the order of one centimeter and below the roughness of the surface and perhaps other surface phenomena affect the magnitude of the surface resistance.[1] At millimeter wavelengths the effect of surface roughness becomes very pronounced.

The term "roughness" will be used to describe a surface which has irregularities from a smooth, flat plane. Methods to measure this roughness exist, direct and optical.[2,3] This investigation of the relationship of surface roughness and resistance will use the non-destructive technique of optically measuring the variations. The purpose of this research is to provide a model to correlate surface roughness to surface resistance for the predictions of the power losses at millimeter wavelengths and to find methods of their reduction.

Literature Survey

Abnormally low values of Q were reported by several investigators in the 1940's and 1950's. Morgan[4] reported that at frequencies above 10,000 MHz the calculated Q's were much higher than measured experimentally. Horner et al[5] observed the same at measurements on cavity resonators at frequencies near 3,000 MHz. However, Gevers reported Q-value measurements at 3,000 MHz which were 98% of the theoretical value when using a precision lathe and diamond tools to give surface variations of only about 10^{-3} microns. Dr. F. A. Benson[1] investigated surface roughness effects on waveguide attenuation. As a result of their work at centimeter wavelengths, Dr. Benson modified the attenuation constant expression, derived by S. Kuhn,[6] to account for the surface variation.

To determine the surface variation two techniques have been used. A stylus-type instrument records the up and down vertical motion of a sharp needle as it travels along the surface. As a second method, the surface can be cut cross-sectionally and the edge viewed under a powerful microscope. But the most recent technique of studying surface roughness is based on light reflectance from the rough surface. Dr. H. E. Bennett and Dr. J. O. Porteus published a number of papers on relationships of surface roughness and specular reflection at near normal incidence in the early 1960's. Their work was based on earlier publication of H. Davies, "The Reflection of Electromagnetic Waves from a Rough Surface." Davies' expression for specular reflection was based on the assumption of a perfectly conducting surface and that the

root mean square deviation of the surface from the mean surface level is small compared with the wavelength. Bennett and Porteus modified Davies' expression by multiplying the reflectance from rough, perfectly conducting surfaces by the reflectance of a smooth surface of the actual material.

Dr. K. E. Torrance and Dr. E. M. Sparrow in recent years have studied reflections from rough surfaces when the root mean square deviation of the surface from the mean surface level is of the order of or greater than a wavelength. Their theory is based on geometrical optics.

The literature search continues at this time.

Investigation

As an initial step in the investigation, it was important to determine the feasibility of measuring surface roughness. Several rectangular blocks of copper were cut for the test specimens. Roughness was created by grinding which leaves the prepared surface with parallel grooves with random depth. Each copper specimen was ground on a different grade of abrasive paper which results in a difference in maximum surface deviations. Each specimen was cut cross-sectionally, revealing an edge view of the surface. To facilitate the observation, the cut specimens are molded into a cylinder of bakelit and the exposed surface polished. The polishing removes the foreign material and fragmented metal caused by the cutting operation. The amount of material removed was between 0.4 and 0.5 mm. Then the surfaces were viewed through a microscope, Bausch and Lomb, Serial Number SE 176, Metallograph.

The microscope has magnification powers ranging from 70 to 2,150 times the actual size. An eyepiece with a movable cross-hair was calibrated with a precision incremented strip. A comparison between surfaces was made by measuring displacement between the highest and lowest points of the surfaces for each of three grades of surface roughness. The smoothest surface variation was 1.9 μ, the next was 3.9 μ, and the roughest was 13.8 μ. These measurements covered a section of surface approximately 500 μ in length. A record of the roughest surface was made by photographing through the microscope the image onto metallographic plates. The image of the surface was then enlarged and printed on photographic paper. The process provided an approximate surface magnification of 250. From the photographic print, the surface deviations were taken and were 14.2 μ compared to 13.8 μ by direct observation.

Attempts to improve the observations of the surface structure by nickel plating gave very little discernible improvement.

Figures 4.1 and 4.2 show specimens of blocks of copper embedded in plastic and bakelit and a copy of the photograph of the roughest surface structure. One part of the scale on Fig. 4.2 represents 25.4 μ.

Plan of Work

The investigation will have several parts. One will deal with the determination of roughness of metallic surfaces by measuring the distribution of light reflectance and the technique will be verified by microscopic observations. Measurements of Q-values of test cavities at millimeter wavelengths will give

the surface resistance of the evaluated surfaces which then will be related to the measured surface roughness. The wall roughness of the various cavities will be created by using different grit sizes of abrasive material. A model will then be developed of the electromagnetic surface effects and relationships will be found between surface resistance and roughness. The derived relationships and procedures will then be used for the comparison of cavities with surfaces treated in various ways to reduce the surface resistance. The results will be used for the preparation of the walls of waveguides with reduced attenuation.

References

1 F. A. Benson, Waveguide Attenuation and Its Correlation with Surface Roughness, IEE Proc, Part 3, 101:12, p. 85-90, 1952

2 H. E. Bennett and J. O. Porteus, Relation Between Surface Roughness and Specular Reflectance at Normal Incidence, J. Opt. Soc. Am., 51:2, p. 123-129, 1961

3 K. E. Torrance and E. M. Sparrow, Theory of Off-Specular Reflection from Roughened Surfaces, J. Opt. Soc. Am., 57:9, p. 1102-1114, 1967

4 S. P. Morgan, Effect of Surface Roughness on Eddy Current Losses at Microwave Frequencies, J. Appl. Phys., 20, p. 352, 1949

5 F. Horner, T. A. Taylor, R. Dunsmuir, J. Lamb, and W. Jackson, Resonance Methods of Dielectric Measurements at Centimetre Wavelengths, Journal IEE, Part 3, 93, p. 53, 1946

6 S. Kuhn, Calculation of Attenuation in Waveghides, Journal IEE, Part 3, 93, p. 663-678, 1946

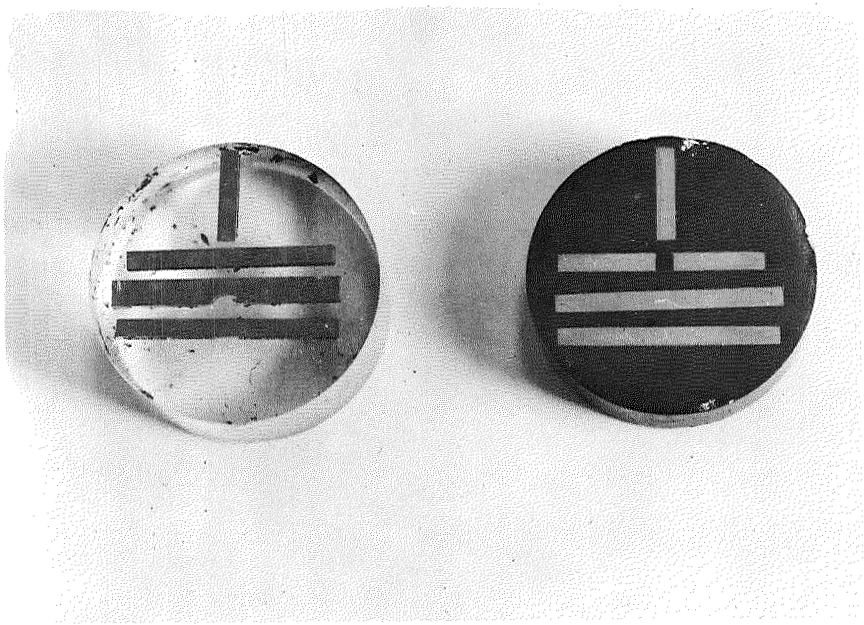

Fig. 4.1 Specimens of copper walls embedded in plastic and bakelite. Polished cross sections for three grades of surface roughness are shown.

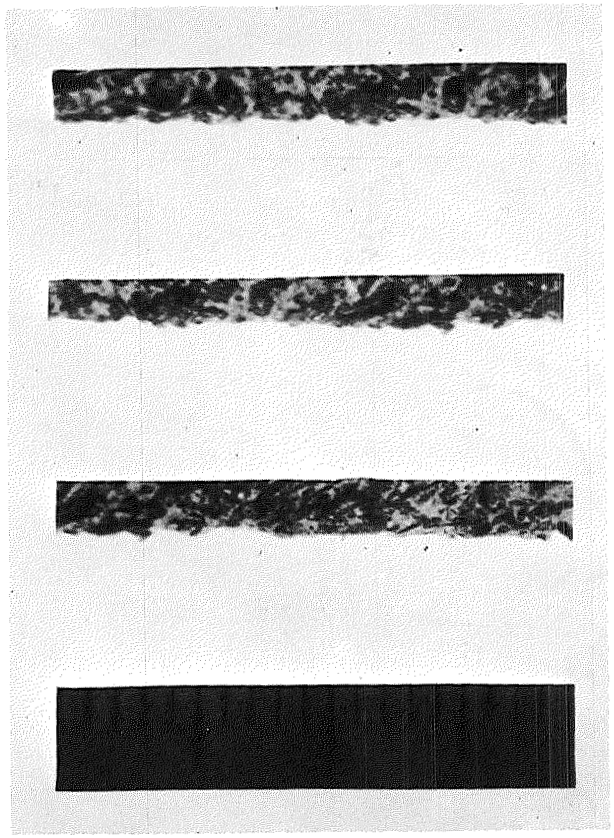

Fig. 4.2 Microphotograph of cross-sectional views for maximum roughness. One part of the scale on top equals 25.4 μm.

Part 5

FIELD DISTRIBUTIONS IN FRONT OF H-GUIDE HORN TRANSITIONS

Abstract

A newly designed horn-type transition between rectangular waveguides and fence guides and coupling plates are described. The field distributions measured in front of the horn and the coupling elements are shown in diagram form.

FIELD DISTRIBUTIONS IN FRONT OF H-GUIDE HORN TRANSITIONS

At the experimental study of H-guides and fence guides, several types of coupling elements are used at present between these guides and rectangular waveguides. These coupling elements represent shorts if short sections of the above guides are used as resonators and may serve as mode transformers between the rectangular guides and the other guides. A special horn-type transition was designed to be used for the mode conversion with minimum discontinuities and high efficiency. It consists of a horn-type structure with the upper and lower surfaces of the rectangular waveguide flaring up to form the horn. In the center, a dielectric slab concentrates the field in its vicinity and generates at the horn amperture a field distribution corresponding to that of the H-guide or fence guide. Figure 5.1 shows a photograph of the structure. If the fence-guide section is used as a resonator, a one-dimensional, multi-hole coupler, shown on the right-hand side of the figure, is inserted between the horn and the guide.

The field distribution in front of the horn was measured under various conditions to assure proper operation if used for the indicated purposes. The following figures show sketches of the conditions under which the measurements were made. Figure 5.2 shows a single-hole coupler directly attached to a rectangular waveguide to be used for resonators consisting of sections of fence guide and H-guide. The field distribution in front of the single-horn coupler at various distances is shown

in diagram form in Fig. 5.6. Such a coupler generates an excessive number of undesired modes. Figure 5.3 illustrates the multi-hole coupler which, if used in a resonator, generates a field distribution of the fundamental mode and suppresses undesired modes. The field distribution in front of the structure is shown in Fig. 5.7. Figure 5.8 presents the field distribution in front of the horn without coupling plates which is uniform as predicted. In the presence of a dielectric slab the field distribution is characterized by a predominantly exponential decrease of the fields from the center of the horn typical of the H-guide mode. Measured diagrams are shown in Fig. 5.9. The geometrical configuration of the horn is illustrated in Fig. 5.4. A double-slab structure is shown in Fig. 5.5 and its field distribution shows a field decrease from the center toward the upper and lower walls similar to that of the single-slab horn. The probe used for the field measurements will be described in a later report. Measurements for the determination of the discontinuities introduced by the transition are underway at present.

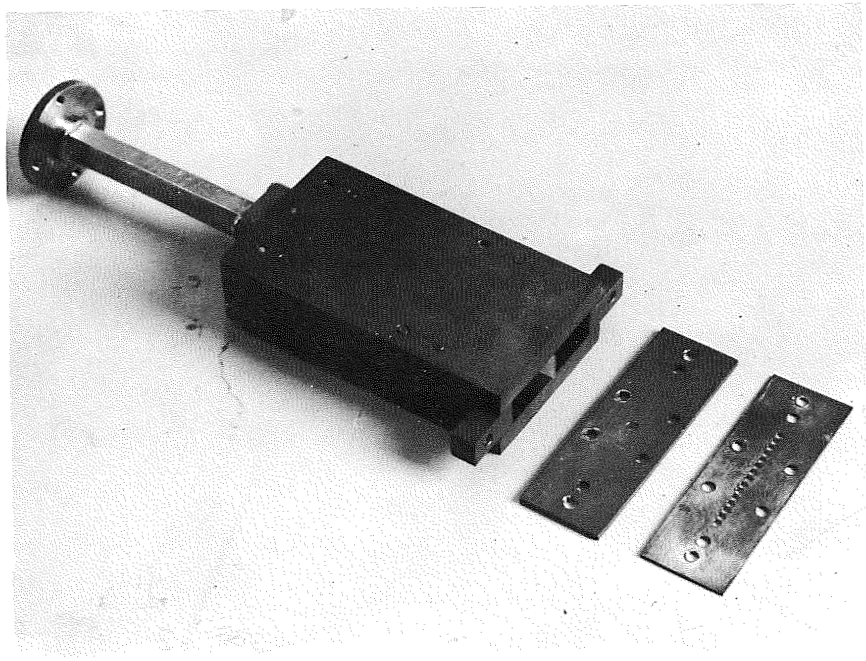

Fig. 5.1 Wave-mode transformer and coupling plates.

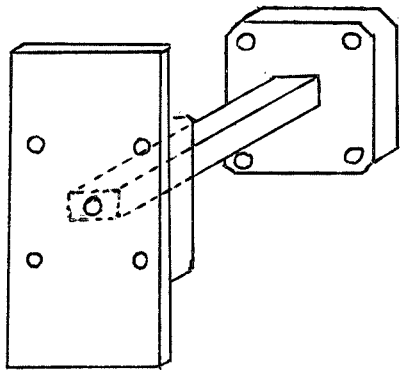

Fig. 5.2 Single-hole coupler

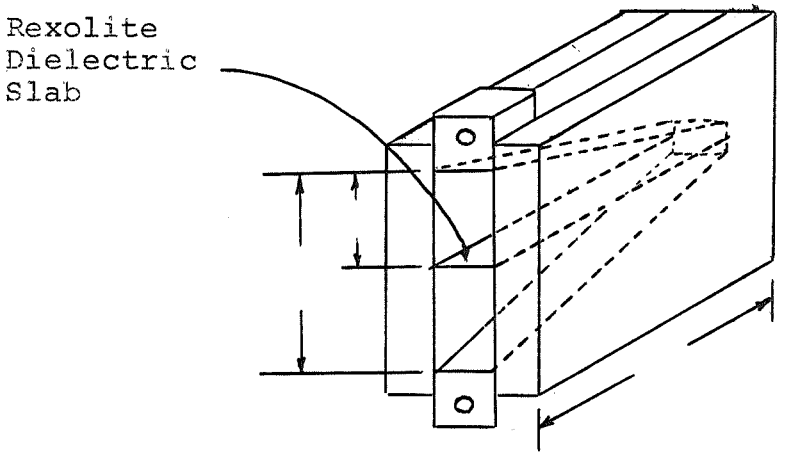

Fig. 5.4 Horn transition with single slab

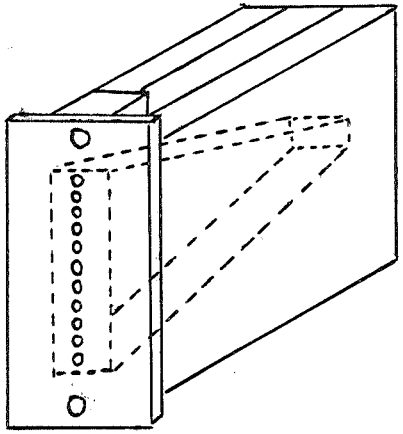

Fig. 5.3 Multiple-hole coupler

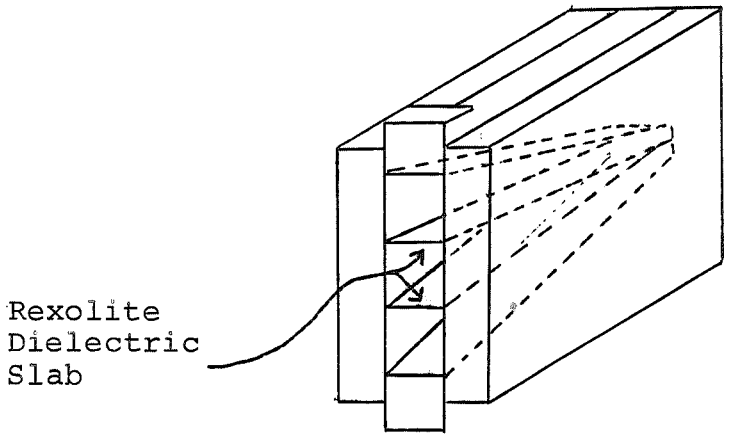

Fig. 5.5 Horn transition with double slab

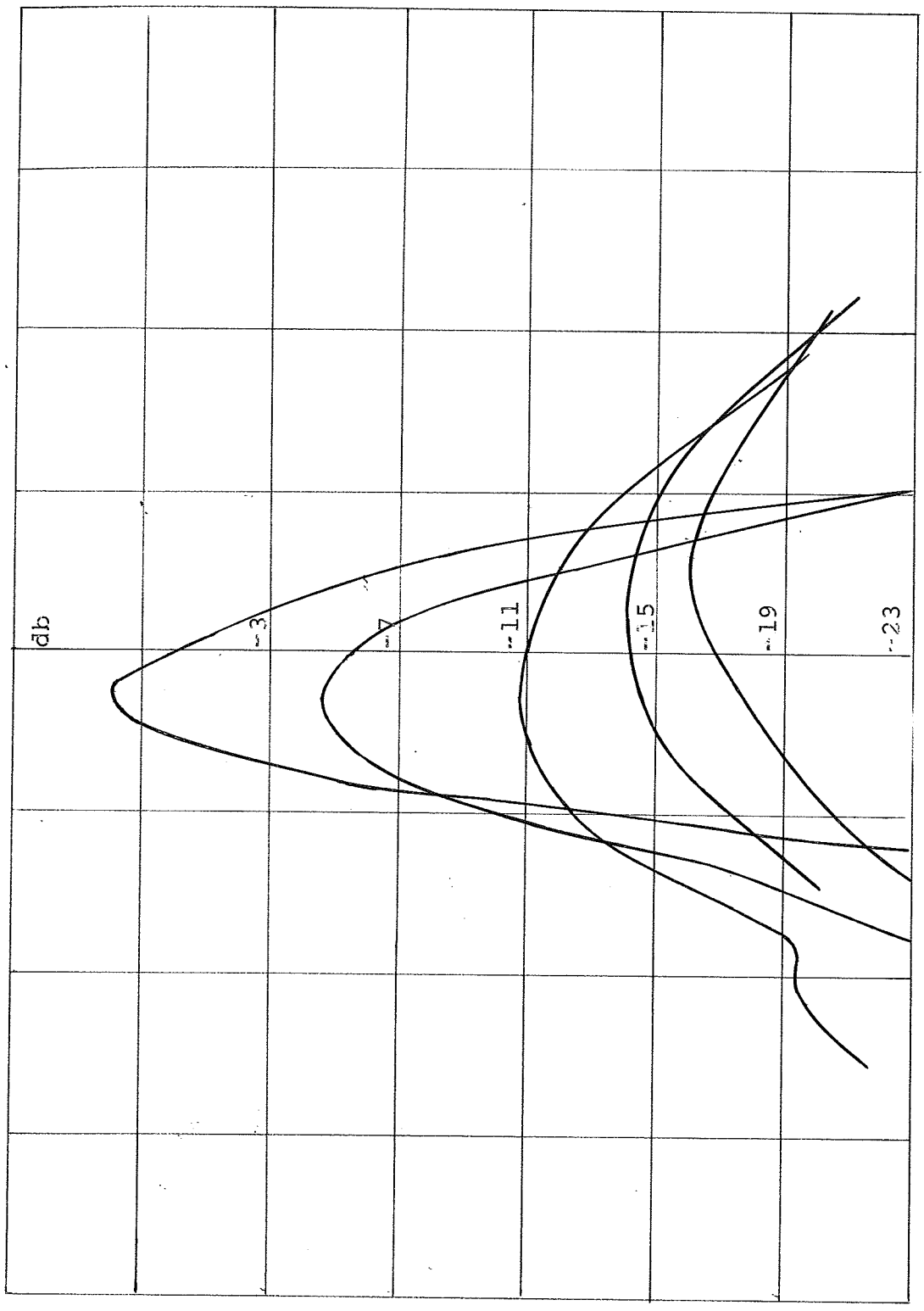

Fig. 5.6 Field in front of single-hole coupler (Fig. 5.2)

← → Distance above and below center

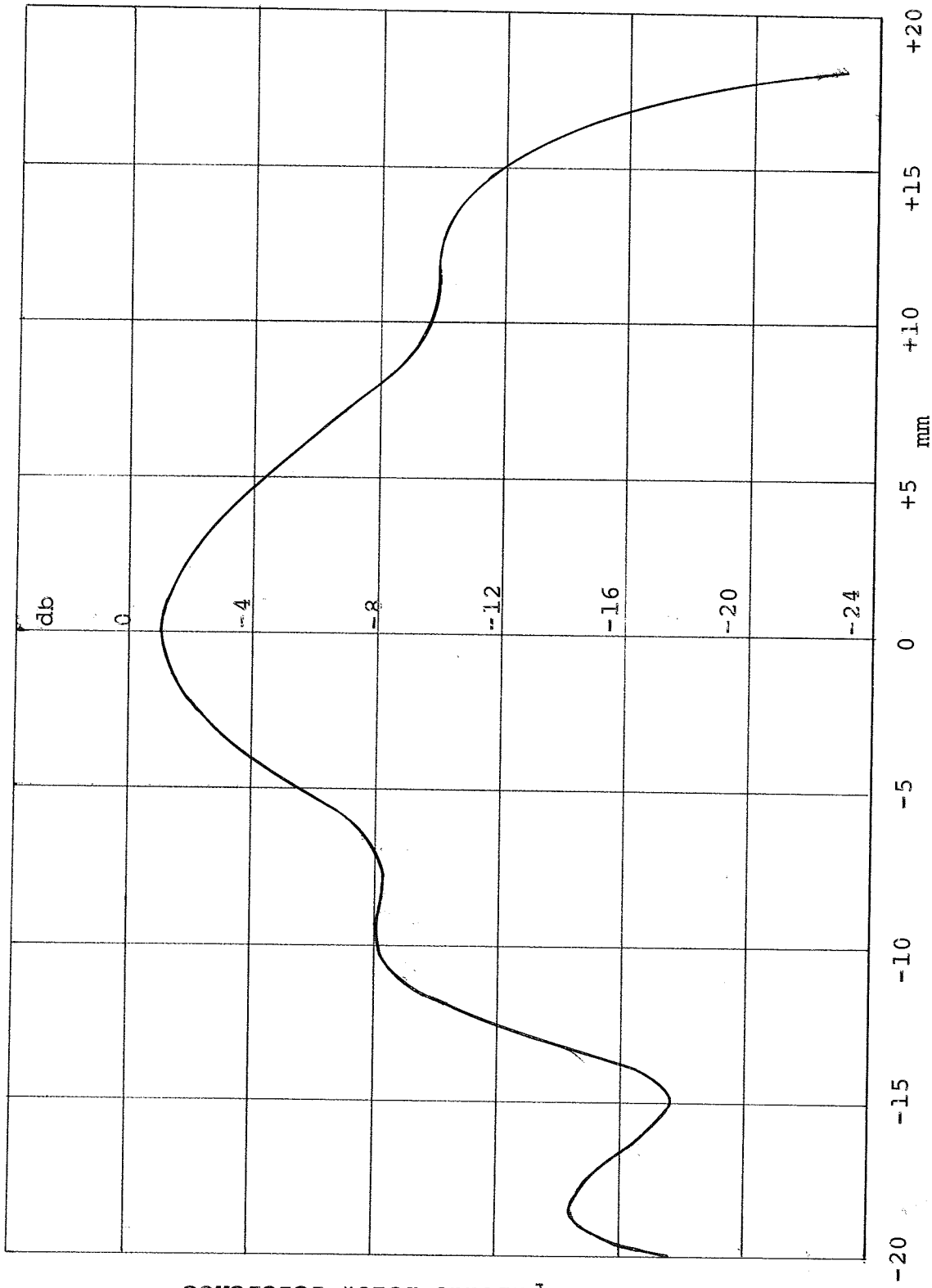

Fig. 5.7 Field in front of multi-hole coupler (Fig. 5.3)

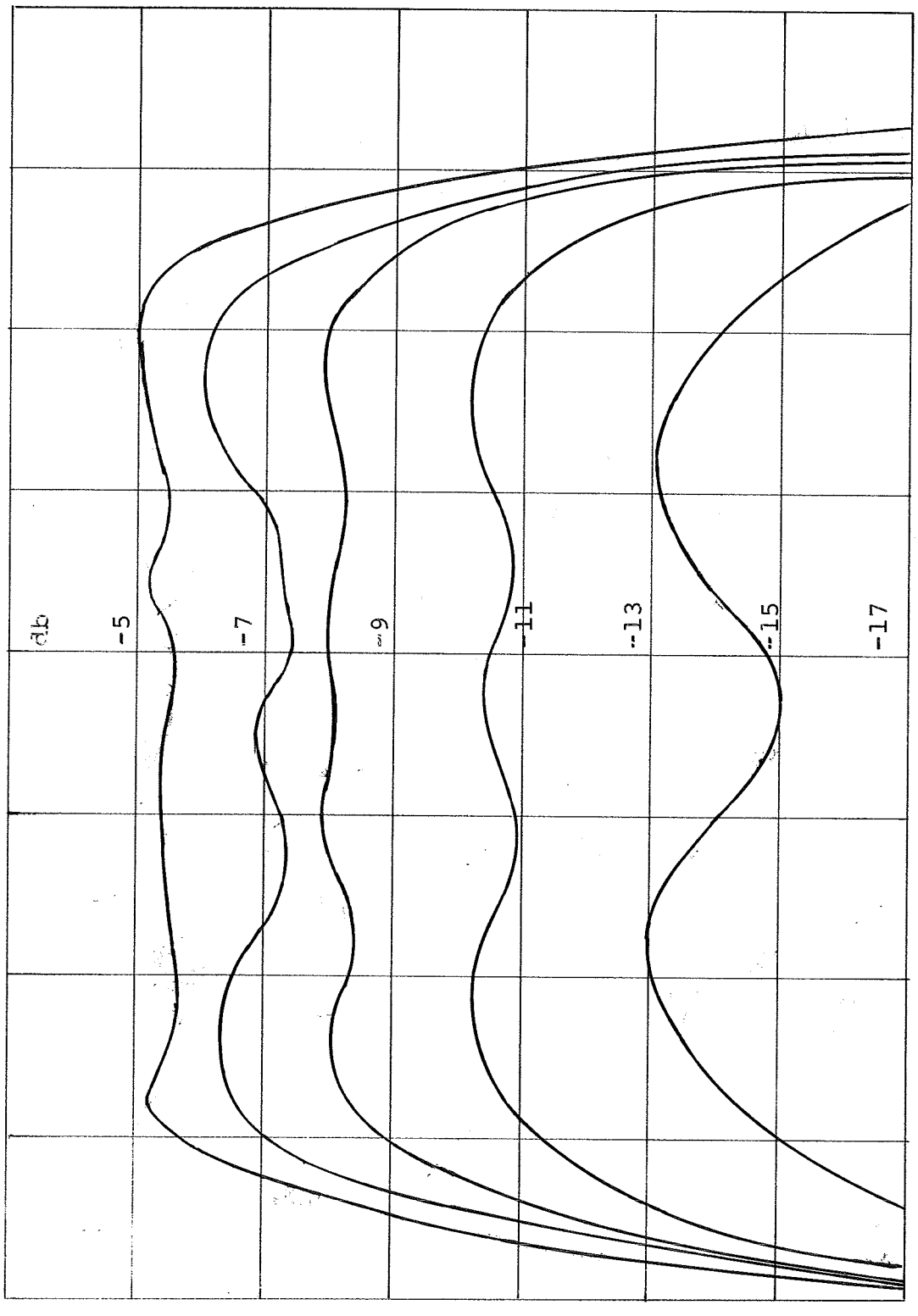

Fig. 5.8 Field in front of empty horn

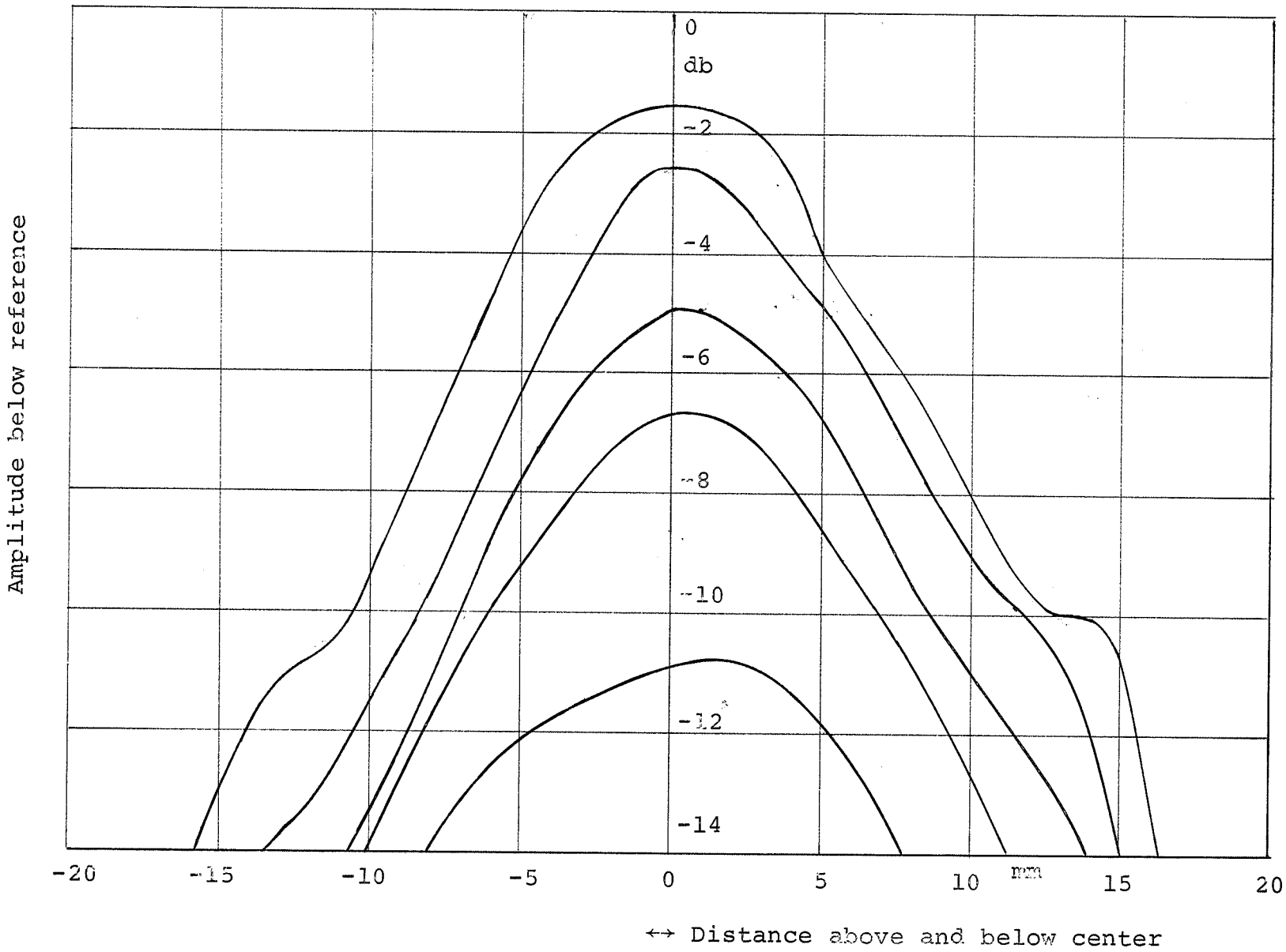

Fig. 5.9 Field in front of horn with dielectric strip (Fig. 5.4)

Part 6

THE CHARACTERISTICS OF BICOMPLEX WAVE-ANALYTIC FUNCTIONS

Abstract

The present part completes the description of the commutative bicomplex number system. It continues with a consideration of bicomplex analytic and wave-analytic functions. The latter are derived from expanded Cauchy-Riemann equations. It is shown that these functions satisfy under certain conditions the wave equation (Helmholtz' equation).

5. Reflexion and Adjoint Operator

With respect to a given b.c. operator

$$\zeta = \zeta_1 + j\,\zeta_2 \simeq \begin{bmatrix} \zeta_{11} & -\zeta_{12} \\ \zeta_{21} & \zeta_{22} \end{bmatrix} \qquad (5.1)$$

we consider the following b.c. operator:

$$\zeta^x \triangleq j^{-1}\,\zeta j = \begin{bmatrix} 0 & 1 \\ -1 & 0 \end{bmatrix} \begin{bmatrix} \zeta_{11} & -\zeta_{12} \\ \zeta_{21} & \zeta_{22} \end{bmatrix} \begin{bmatrix} 0 & -1 \\ 1 & 0 \end{bmatrix}$$

$$= \begin{bmatrix} \zeta_{22} & -\zeta_{21} \\ \zeta_{12} & \zeta_{11} \end{bmatrix} \qquad (5.2)$$

This operator ζ^x will be called the "reflexion operator" of ζ. In particular, we have

$$\zeta_1{}^x \triangleq j^{-1}\,\zeta_1 j = \begin{bmatrix} \zeta_{22} & 0 \\ 0 & \zeta_{11} \end{bmatrix}$$

$$\zeta_2{}^x = j^{-1}\,\zeta_2 j = \begin{bmatrix} \zeta_{12} & 0 \\ 0 & \zeta_{21} \end{bmatrix} \qquad (5.3)$$

Accordingly,

$$\zeta^x = j^{-1}\,(\zeta_1 + j\,\zeta_2)\,j = (j^{-1}\,\zeta_1 j) + j(j^{-1}\,\zeta_2 j)$$

$$= \zeta_1{}^x + j\,\zeta_2{}^x \qquad (5.4)$$

Obviously, we have

$$\zeta^{xx} = \zeta$$

Next we define the "adjoint operator" of ζ as follows:

$$\zeta^* \triangleq \zeta_1{}^x - j\zeta_2 = \begin{bmatrix} \zeta_{22} & \zeta_{12} \\ -\zeta_{22} & \zeta_{11} \end{bmatrix} \qquad (5.6)$$

This represents the adjoint matrix of ζ.

From the above definition we obtain

$$\zeta\zeta^* = (\zeta_1 + j\,\zeta_2)\,(\zeta_1{}^x - j\,\zeta_2)$$

$$= \zeta_1\zeta_1{}^x + j\zeta_2\,\zeta_1{}^x - \zeta_1 j\zeta_2 - j\zeta_2 j\zeta_2$$

$$= \zeta_1\zeta_1{}^x + j(\zeta_2\zeta_1{}^x - \zeta_1{}^x\,\zeta_2) + \zeta_2{}^x\,\zeta_2 \qquad (5.7)$$

and since $\zeta_1{}^x$ and ζ_2 are both diagonal matrices, they are cummutative; i.e.,

$$\zeta_1{}^x\,\zeta_2 = \zeta_2\,\zeta_1{}^x$$

so that the second term of Eq. (5.7) vanishes and we get

$$\zeta\zeta^* = \zeta_1\zeta_1{}^x + \zeta_2{}^x\,\zeta_2$$

$$= \begin{bmatrix} \zeta_{11} & \zeta_{22} & 0 & \\ & 0 & \zeta_{22} & \zeta_{11} \end{bmatrix} + \begin{bmatrix} \zeta_{12} & \zeta_{21} & 0 & \\ & 0 & \zeta_{21} & \zeta_{12} \end{bmatrix}$$

$$= \begin{bmatrix} \zeta_{11}\,\zeta_{22} + \zeta_{12}\,\zeta_{21} & & 0 & \\ & 0 & & \zeta_{11}\,\zeta_{22} + \zeta_{21}\,\zeta_{12} \end{bmatrix}$$

$$\simeq \zeta_{11}\ \zeta_{22} + \zeta_{21}\ \zeta_{12} = \det \zeta \quad . \qquad (5.8)$$

Therefore, the product $\zeta\zeta^*$ represents the determinant of ζ which we denote for convenience

$$\overset{\circ}{\zeta}{}^2 \triangleq \det \zeta = \zeta\zeta^+ = \zeta_1\ \zeta_1{}^x + \zeta_2\ \zeta_2{}^x \qquad (5.9)$$

From this relation we know the inverse operator ζ^{-1} of ζ is given by

$$\zeta^{-1} = \zeta^* / \overset{\circ}{\zeta}{}^2 \qquad (5.10)$$

provided $\overset{\circ}{\zeta}{}^2 = \det \zeta \neq 0$.

It can easily be seen that the adjoint operator ζ^* has also the following properties:

$$\begin{cases} \zeta + \zeta^* \simeq \zeta_{11} + \zeta_{22} = \text{trace of } \zeta \quad . & (5.11) \\ (\zeta^*)^* = \zeta & (5.12) \end{cases}$$

and if ζ and η are two b.c. operators, then

$$\underline{(\zeta\eta)^* = \eta^*\zeta^*} \qquad (5.13)$$

For

$$\zeta\,\eta = (\zeta_1 + j\,\zeta_2)\ (\eta_1 + j\,\eta_2)$$

$$= (\zeta_1\,\eta_1 - \zeta_2{}^x\,\eta_2) + j\,(\zeta_2\,\eta_1 + \zeta_1{}^x\,\eta_2) \qquad (5.14)$$

Therefore

$$(\zeta\,\eta)^* = (\zeta_1\eta_1 - \zeta_2{}^x\,\eta_2)^x - j(\zeta_2\eta_1 + \zeta_1{}^x\,\eta_2)$$

$$= (\zeta_1{}^x\,\eta_1{}^x - \zeta_2\eta_2{}^x) - j(\zeta_2\,\eta_1 + \zeta_1{}^x\,\eta_2) \qquad (5.15)$$

On the other hand

$$\eta^* \zeta^* = (\eta_1^x - j\eta_2)\ (\zeta_1^x - j\zeta_2)$$

$$= (\eta_1^x \zeta_1^x - \eta_2^x \zeta_2) - j(\eta_1 \zeta_2 + \eta_2 \zeta_1^x) \qquad (5.16)$$

Comparing Eq. (5.15) and Eq. (5.16), we get Eq. (5.13) .

6. B. C. Analytic (Holomorphic) Function

Let $w_1(Z_1 , Z_2)$ and $w_2(Z_1 , Z_2)$ be two complex functions of two complex variables Z_1 and Z_2 . If both w_1 and w_2 are analytic with respect to Z_1 and Z_2 in the complex domains $D_1(Z_1)$ and $D_2(Z_2)$, respectively, and satisfy the complex Cauchy-Riemann equations:

$$\begin{cases} \dfrac{\partial w_1}{\partial Z_1} - \dfrac{\partial w_2}{\partial Z_2} = 0 & (6.1) \\ \dfrac{\partial w_1}{\partial Z_2} + \dfrac{\partial w_2}{\partial Z_1} = 0 & (6.2) \end{cases}$$

then the bicomplex function $w = w_1 + jw_2$ will be called a bicomplex analytic or holomorphic function of the single b.c. variable $Z = Z_1 + jZ_2$ in the b.c. domain $D = D_1 \times D_2$.

Making use of the notations:

$$\partial_1 \stackrel{D}{=} \frac{\partial}{\partial Z_1} \qquad \text{and} \qquad \partial_2 \stackrel{D}{=} \frac{\partial}{\partial Z_2} \tag{6.3}$$

the above (6.1) and (6.2) are written as

$$\begin{cases} \partial_1 w_1 - \partial_2 w_2 = 0 & (6.1)' \\ \partial_2 w_1 + \partial_1 w_2 = 0 & (6.2)' \end{cases}$$

These two equations are unified in the following complex vectorial equation:

$$\begin{bmatrix} \partial_1 & -\partial_2 \\ \partial_2 & \partial_1 \end{bmatrix} \begin{bmatrix} w_1 \\ w_2 \end{bmatrix} = 0 \tag{6.4}$$

This can be written simply as

$$\boxed{\nabla w = 0} \qquad (6.5)$$

where

$$\nabla \triangleq \begin{bmatrix} \partial_1 & -\partial_2 \\ \partial_2 & \partial_1 \end{bmatrix} = \begin{bmatrix} \partial_1 & 0 \\ 0 & \partial_1 \end{bmatrix} + \begin{bmatrix} 0 & -1 \\ 1 & 0 \end{bmatrix} \begin{bmatrix} \partial_2 & 0 \\ 0 & \partial_2 \end{bmatrix}$$

$$\simeq \partial_1 + j\partial_2 \qquad (6.6)$$

and by (1.14)

$$w \triangleq \begin{bmatrix} w_1 \\ w_2 \end{bmatrix} = \begin{bmatrix} w_1 \\ 0 \end{bmatrix} + \begin{bmatrix} 0 & -1 \\ 1 & 0 \end{bmatrix} \begin{bmatrix} w_2 \\ 0 \end{bmatrix}$$

$$\simeq w_1 + jw_2 \qquad (6.7)$$

The above Eq. (6.5) is the unified form of the complex Cauchy-Riemann Eqs. (6.1) and (6.2).

If we change the sign of w_2 in Eqs. (6.1) and (6.2), we get the conjugate Cauchy-Riemann equations:

$$\begin{cases} \partial_1 w_1 + \partial_2 w_2 = 0 \\ \partial_2 w_1 - \partial_1 w_2 = 0 \end{cases} \qquad (6.8)$$

These can be unified into

$$\boxed{\nabla^* w^* = 0}$$

where

$$\begin{cases} \nabla^* \triangleq \tilde{\nabla} = \partial_1 - j\partial_2 \\ w^* \triangleq \tilde{w} = w_1 - jw_2 \end{cases}$$

The above Eq. (6.9) may be obtained directly from Eq. (6.5) by simply changing the sign of j.

Since

$$\nabla^*\nabla = (\partial_1 - j\partial_2)(\partial_1 + j\partial_2) = \partial_1^2 + \partial_2^2 \stackrel{D}{=} \Delta \text{ (Laplacian)}$$

$$= \partial_1^2 + \partial_2^2 \stackrel{D}{=} \Delta \text{ (two-dimensional Laplacian)}$$

$$= \nabla\nabla^* \qquad (6.11)$$

we obtain from Eqs. (6.5) and (6.9) by operating ∇^* and ∇, respectively, from the left,

$$\Delta w = \Delta w^* = 0 \qquad (6.12)$$

which shows that both w and w^* are b.c. harmonic functions. The converse is not true, i.e., a b.c. harmonic function u(z) does not necesarily satisfy Eqs. (6.5) or (6.9). However, we have the following

Decomposition Theorem. Any b.c. harmonic function u(z) can be decomposed into a sum of a b.c. analytic function w(z) and its conjugate function $\tilde{w}(z)$.

Proof. Suppose a b.c. function $u(z) = u_1(z) + ju_2(z)$ satisfy in a b.c. domain $D = D_1 \times D_2$ the two dimensional Laplace equation:

$$\Delta u = 0 \qquad (6.13)$$

Since $\Delta u = \Delta u_1 + j\Delta u_2 = 0$, each of the component complex functions $u_1(z)$ and $u_2(z)$ should satisfy the two-dimensional Laplace equation, i.e.,

$$\Delta u_1 = 0 \quad \text{and} \quad \Delta u_2 = 0 \qquad (6.14)$$

But these are precisely the integrability conditions, i.e., the necessary and sufficient conditions for the existence of the two other complex functions $v_1(z)$ and $v_2(z)$ such that in the b.c. domain $D = D_1 \times D_2$ of $Z = Z_1 + jZ_2$, the Cauchy-Riemann equations hold:

$$\begin{cases} \partial_1 u_1 - \partial_2 v_1 = 0 \\ \partial_2 u_1 - \partial_2 v_1 = 0 \end{cases} \qquad (6.15)_1$$

and

$$\begin{cases} \partial_1 u_2 + \partial_2 v_2 = 0 \\ \partial_2 u_2 - \partial_1 v_2 = 0 \end{cases} \qquad (6.15)_2$$

Therefore, the b.c. functions

$$w_1 = u_1 + jv_1 \qquad \text{and} \qquad w_2 = v_2 + ju_2 \qquad (6.16)$$

are b.c. analytic in the domain $D = D_1 \times D_2$, i.e., they satisfy

$$\nabla w_1 = 0 \qquad \text{and } \nabla w_2 = 0 \qquad (6.17)$$

The b.c. j-conjugate functions of w_1 and w_2 are given by

$$\tilde{w}_1 = u_1 - jv_1 \qquad \text{and} \qquad \tilde{w}_2 = v_2 - ju_2 \qquad (6.18)$$

From Eqs. (5.16) and (5.18) we have

$$\begin{cases} u_1 = \frac{1}{2} (w_1 + \tilde{w}_1) \\ u_2 = \frac{1}{2j} (w_2 - \tilde{w}_2) \end{cases} \qquad (6.19)$$

Hence,

$$u = j_1 + ju_2 = \frac{1}{2}(w_1 + \tilde{w}_1) + \frac{1}{2}(w_2 - \tilde{w}_2)$$

$$= \frac{1}{2}(w_1 + w_2) + \frac{1}{2}(\tilde{w}_1 - \tilde{w}_2)$$

$$= w + \tilde{w}$$

where

$$\begin{cases} w \triangleq \frac{1}{2}(w_1 + w_2) \\ \tilde{w} \triangleq \frac{1}{2}(\tilde{w}_1 + \tilde{w}_2) \end{cases} \qquad (6.20)$$

Thus, we have proved that any b.c. harmonic function u can be decomposed into the sum of a b.c. analytic function w and its conjugate function $\tilde{w}$.

7. B. C. Wave-Analytic Function

Suppose two complex functions $w_1(Z_1 , Z_2)$ and $w_2(Z_1 , Z_2)$ of two complex variables Z_1 and Z_2 satisfy instead of Eqs. (6.1) and (6.2) the following set of partial differential equations:

$$\begin{cases} \partial_1 w_1 - \partial_2 w_2 = \zeta_{11} w_1 - \zeta_{12} w_2 & (7.1) \\ \partial_2 w_1 + \partial_1 w_2 = \zeta_{21} w_1 + \zeta_{22} w_2 & (7.2) \end{cases}$$

These two equations can be put together in a single equation:

$$\begin{bmatrix} \partial_1 & -\partial_2 \\ \partial_2 & \partial_1 \end{bmatrix} \begin{bmatrix} w_1 \\ w_2 \end{bmatrix} = \begin{bmatrix} \zeta_{11} & -\zeta_{12} \\ \zeta_{21} & \zeta_{22} \end{bmatrix} \begin{bmatrix} w_1 \\ w_2 \end{bmatrix} \qquad (7.3)$$

If we write as before

$$\begin{cases} \nabla \triangleq \begin{bmatrix} \partial_1 & -\partial_2 \\ \partial_2 & \partial_1 \end{bmatrix} = \partial_1 + j\partial_2 & (7.4) \\ \zeta \triangleq \begin{bmatrix} \zeta_{11} & -\zeta_{12} \\ \zeta_{21} & \zeta_{22} \end{bmatrix} = \zeta_1 + j\zeta_2 & (7.5) \end{cases}$$

where

$$\zeta_1 \triangleq \begin{bmatrix} \zeta_{11} & -0 \\ 0 & \zeta_{22} \end{bmatrix} \quad \text{and} \quad \zeta_2 \triangleq \begin{bmatrix} \zeta_{21} & 0 \\ 0 & \zeta_{12} \end{bmatrix} \qquad (7.6)$$

and

$$w \triangleq \begin{bmatrix} w_1 \\ w_2 \end{bmatrix} = w_1 + jw_2 \qquad (7.7)$$

The above Eq. (7.3) is written simply as

$$\boxed{\nabla w = \zeta w} \qquad (7.8)$$

or

$$(\nabla - \zeta)\, w = 0 \qquad (7.8)'$$

A b.c. function w which satisfied Eqs. (7.8) or (7.8)' at every point $Z \varepsilon D$ will be called "b.c. wave-analytic" in the b.c. domain $D = D_1 \times D_2$. In particular, when $\zeta = 0$, the Eq. (7.8) reduces to the b.c. Cauchy-Riemann Eq. (6.5).

In the following we shall assume $\zeta \neq 0$ and to be constant in the domain D.

If we operate the adjoint operator $(\nabla^* - \zeta^*)$ of $(\nabla - \zeta)$ on Eq. (7.8)' , we obtain

$$(\nabla^* - \zeta^*)(\nabla - \zeta)\, w = 0 \qquad (7.9)$$

Now

$$(\nabla^* - \zeta^*)(\nabla - \zeta) = \nabla^*\nabla - (\zeta^*\nabla + \nabla^*\zeta) + \zeta^*\zeta \qquad (7.10)$$

From Eqs. (6.11) and (5.8), we have

$$\nabla^*\nabla = \nabla\nabla^* = \Delta$$

$$\zeta^*\zeta = (\zeta_1^{\times} - j\zeta_2)\,(\zeta_1 + j\zeta_2)$$

$$= \zeta_1^{\times}\,\zeta_1 + \zeta_2^{\times} \simeq \zeta_{11}\,\zeta_{22} + \zeta_{21}\,\zeta_{12}$$

$$= \det \zeta \triangleq {}^{02}\zeta \qquad (7.11)$$

and

$$(\zeta^{*}\nabla + \nabla^{*}\zeta) = (\zeta_1{}^{x} - j\zeta_2)(\partial_1 + j\partial_2) + (\partial_1 - j\partial_2)(\zeta_1 + j\zeta_2)$$

$$= (\zeta_1{}^{x}\,\partial_1 - j\zeta_2\,\partial_1 + \zeta_1{}^{x}\,j\partial_2 - j\zeta_2\,j\partial_2)$$

$$+ (\partial_1\zeta_1 - j\partial_2\zeta_1 + \partial_1 j\zeta_2 - j\partial_2 j\zeta_2) \qquad (7.12)$$

Since ζ_1 and ζ_2 are assumed to be constant, we have

$$\partial_i\zeta_j = \zeta_j\partial_i \quad (i\ ,\ j = 1,\ 2) \quad .$$

Also by Eq. (5.3)

$$\zeta_i{}^{x}\ j = j\zeta_i \quad (i = 1,\ 2) \quad . \qquad (7.13)$$

By making use of these relations, we get

$$(7.12) = (\zeta_1{}^{x} + \zeta_1)\ \partial_1 + (\zeta_2{}^{x} + \zeta_2)\ \partial_2$$

$$\simeq (\zeta_{11} + \zeta_{22})\ \partial_1 + (\zeta_{21} + \zeta_{12})\ \partial_2 \qquad (7.14)$$

Therefore, Eq. (7.9) becomes

$$\Delta w = \{(\zeta_{11} + \zeta_{22})\ \partial_1 + (\zeta_{21} + \zeta_{12})\ \partial_2\}\ w + \overset{\circ}{\zeta}{}^{2}\ w = 0 \qquad (7.15)$$

This may be written as

$$\Delta w - 2(\zeta_1{}^{+}\partial_1 + \zeta_2{}^{+}\ \partial_2)\ w + \overset{\circ}{\zeta}{}^{2}\ w = 0 \qquad (7.15)'$$

where

$$\begin{cases} \zeta_1{}^{+} \triangleq \dfrac{1}{2}\ (\zeta_{11} + \zeta_{22}) \\ \zeta_2{}^{+} \triangleq \dfrac{1}{2}\ (\zeta_{21} + \zeta_{12}) \end{cases} \qquad (7.16)$$

Thus we see all wave-analytic functions for which $\zeta_1{}^{+}$ and $\zeta_2{}^{+}$ are the same, satisfy the same second-order partial differential equation (7.15)' .

In particular if

$$\begin{cases} \zeta_{22} = -\zeta_{11} \\ \zeta_{21} = -\zeta_{12} \end{cases} \qquad \text{i.e.,} \quad \zeta = \begin{bmatrix} \zeta_{11} & -\zeta_{12} \\ -\zeta_{12} & -\zeta_{11} \end{bmatrix} \qquad (7.17)$$

then $\zeta_1^+ = \zeta_2^+ = 0$ and (7.15)' becomes the reduced wave-equation (or Hemholtz' equation)

$$\Delta w + \overset{\circ}{\zeta}^2 w = 0 \qquad (7.18)$$